CORONAVIRUS

Integrated longitudinal immunophenotypic, transcriptional, and repertoire analyses delineate immune responses in patients with COVID-19

Samuele Notarbartolo[1]*[†], Valeria Ranzani[1][†], Alessandra Bandera[2,3,4][†], Paola Gruarin[1][‡], Valeria Bevilacqua[1][‡], Anna Rita Putignano[1,5][‡], Andrea Gobbini[1,6][‡], Eugenia Galeota[1][‡], Cristina Manara[1][‡], Mauro Bombaci[1], Elisa Pesce[1], Elena Zagato[1,5], Andrea Favalli[1], Maria Lucia Sarnicola[1], Serena Curti[1], Mariacristina Crosti[1], Martina Martinovic[1], Tanya Fabbris[1], Federico Marini[7], Lorena Donnici[1], Mariangela Lorenzo[1], Marilena Mancino[1], Riccardo Ungaro[2], Andrea Lombardi[2], Davide Mangioni[2], Antonio Muscatello[2], Stefano Aliberti[3,8][§], Francesco Blasi[3,8], Tullia De Feo[9], Daniele Prati[10], Lara Manganaro[1], Francesca Granucci[1,6], Antonio Lanzavecchia[1], Raffaele De Francesco[1,11], Andrea Gori[2,3,4], Renata Grifantini[1]*[||], Sergio Abrignani[1,5]*[||]

To understand how a protective immune response against SARS-CoV-2 develops over time, we integrated phenotypic, transcriptional, and repertoire analyses on PBMCs from patients with mild and severe COVID-19 during and after infection and compared them to healthy donors (HDs). A type I IFN response signature marked all the immune populations from severe patients during the infection. Humoral immunity was dominated by IgG production primarily against the RBD and N proteins, with neutralizing antibody titers increasing after infection and with disease severity. Memory B cells, including an atypical FCRL5$^+$ T-BET$^+$ memory subset, increased during the infection, especially in patients with mild disease. A significant reduction of effector memory CD8$^+$ T cells frequency characterized patients with severe disease. Despite such impairment, we observed robust clonal expansion of CD8$^+$ T lymphocytes, whereas CD4$^+$ T cells were less expanded and skewed toward T$_{CM}$ and T$_H$2-like phenotypes. MAIT cells were also expanded, but only in patients with mild disease. Terminally differentiated CD8$^+$ GZMB$^+$ effector cells were clonally expanded both during and after the infection, whereas CD8$^+$ GZMK$^+$ lymphocytes were more expanded after infection and represented bona fide memory precursor effector cells. TCR repertoire analysis revealed that only highly proliferating T cell clonotypes, which included SARS-CoV-2–specific cells, were maintained after infection and shared between the CD8$^+$ GZMB$^+$ and GZMK$^+$ subsets. Overall, this study describes the development of immunity against SARS-CoV-2 and identifies an effector CD8$^+$ T cell population with memory precursor–like features.

INTRODUCTION

The beta coronavirus SARS-CoV-2 is the etiologic agent of the coronavirus disease 2019 (COVID-19) pandemic, characterized by influenza-like illness that can eventually progress to interstitial pneumonia, acute respiratory distress syndrome, and death (*1, 2*). COVID-19 has currently affected over 195 million people worldwide

[1]INGM, Istituto Nazionale Genetica Molecolare "Romeo ed Enrica Invernizzi", Milan, Italy. [2]Infectious Diseases Unit, Fondazione IRCCS Ca' Granda Ospedale Maggiore Policlinico, Milan, Italy. [3]Department of Pathophysiology and Transplantation, Università degli Studi di Milano, Milan, Italy. [4]Centre for Multidisciplinary Research in Health Science (MACH), Università degli Studi di Milano, Milan, Italy. [5]Department of Clinical Sciences and Community Health, Università degli Studi di Milano, Milan, Italy. [6]Department of Biotechnology and Biosciences, University of Milano-Bicocca, Milan, Italy. [7]Institute of Medical Biostatistics, Epidemiology and Informatics (IMBEI), University Medical Center, Mainz, Germany. [8]Respiratory Unit and Cystic Fibrosis Adult Center, Fondazione IRCCS Ca' Granda Ospedale Maggiore Policlinico, Milan, Italy. [9]Unità Operativa Complessa (UOC) Coordinamento Trapianti, Fondazione IRCCS Ca' Granda-Ospedale Maggiore Policlinico, Milan, Italy. [10]Fondazione IRCCS Ca' Granda Ospedale Maggiore Policlinico, Department of Transfusion Medicine and Hematology, Milan, Italy. [11]Department of Pharmacological and Biomolecular Sciences, Università degli Studi di Milano, Milan, Italy.
*Corresponding author. Email: notarbartolo@ingm.org (S.N.); abrignani@ingm.org (S.A.); grifantini@ingm.org (R.G.)
†These authors contributed equally to this work.
‡These authors contributed equally to this work.
§Present address: Humanitas University, Department of Biomedical Sciences, Pieve Emanuele, Milan, Italy; IRCCS Humanitas Research Hospital, Rozzano (MI), Italy.
||Supervising senior authors.

and caused around 4 million deaths. Although the infection often occurs with or without mild symptoms, hospitalization is required for about 5 to 15% of infected people, with a mortality rate around 21 to 26% in this group (*2, 3*). Advanced age and comorbidities represent the most relevant risk factors (*1, 3*). One of the prominent features of severe COVID-19 is a potentially lethal systemic inflammation (*4*) probably derived from a dysregulated type I interferon (IFN) response and an excessive release of proinflammatory cytokines [e.g., interleukin-6 (IL-6) and IL-1β] (*5*).

Adaptive immune responses are crucial to terminate SARS-CoV-2 infection within a few weeks in the great majority of infected individuals. Both cellular and humoral immune responses against SARS-CoV-2 are detected in convalescent individuals, made by CD4$^+$ and CD8$^+$ T lymphocytes and antibodies specific for several viral proteins, such as the nucleoprotein and the spike (S) glycoprotein (*6–10*). The S protein is the main target of neutralizing antibodies. However, the knowledge on the development of a successful immune response in patients with COVID-19 is incomplete and complicated by the occurrence of different patterns of immunological responses correlated with a plethora of covariables (*11–13*).

Here, to improve the understanding of the temporal evolution of the immune response developed by patients successfully dealing with mild or severe COVID-19, we integrated phenotypic, transcriptional, and repertoire analyses at the single-cell level on patients' peripheral

blood mononuclear cells (PBMCs) during the infection and after its resolution. Although circulating immune cells constitute only a small fraction of the total body pool, they are easily accessible and reasonably representative of the ongoing immune response. The analyses performed showed an extensive and durable remodeling of immune cells during and after SARS-CoV-2 infection, characterized by a pervasive type I IFN response, and highlighted a robust $CD8^+$ T cell immune response, defined by the expansion of effector lymphocytes and the generation of memory precursor effector cells (MPECs).

RESULTS

Broad immune remodeling in patients with COVID-19

To assess the dynamics of immune responses elicited by SARS-CoV-2 infection, we collected PBMCs from patients with COVID-19 at the time of acute infection (hereafter indicated as "infection"), namely, within 21 days from the diagnosis, and weeks after the resolution of the infection (hereupon "post-infection"), demonstrated by negative nasopharyngeal swab, after a previous positivity. We investigated innate and adaptive immune responses in 17 patients, 6 with mild disease (no interstitial pneumonia and no oxygen requirement), and 11 with severe disease (pneumonia with respiratory failure) and compared them to 4 healthy individuals [healthy donors (HDs)]. Demographic and clinical characteristics of patients are shown in table S1. The median age of patients was 55 years (interquartile range, 39 to 70), 7 of 17 (41.2%) patients were females, and 11 of 17 (64.7%) had one or more comorbidities. In patients with pneumonia requiring oxygen support, the median PaO2:FiO2 ratio at the time of hospital admission was 200 mmHg. Lymphopenia ($<1 \times 10^9$/liter of lymphocytes) was registered at time of blood collection in 6 of 15 patients [40%; 2 of 17 not available (n/a)]. All patients with mild disease were under 50 years of age, and two of six (33.33%) of them had comorbidities. Nine of 11 (81.81%) of patients with severe disease were over 50 years of age (5 of 11 > 65 years) and 9 of 11 (81.81%) of them had one or more comorbidities, corroborating the knowledge that advanced age and preexisting medical conditions represent the major risk factors for developing a severe disease.

At the two time points, PBMCs were subjected to multiparametric flow cytometry analyses (fig. S1A) and mapped by t-distributed stochastic neighbor embedding (t-SNE) plots (fig. S2A). During the infection, patients with COVID-19, especially those with severe disease, experienced a reduction of T lymphocytes, particularly of $CD8^+$ T cells, and a trend toward increased monocytes proportions, whereas the frequency of B lymphocytes was quite variable (Fig. 1, A and B). On the contrary, natural killer (NK) cells were significantly expanded, especially in individuals with mild disease (Fig. 1A). The proportion of the different PBMC populations tended to normalize post-infection, except for a persistent increased frequency of NK cells.

COVID-19 immune signatures

To identify specific immunological traits of patients with mild or severe disease, during and after the infection, we performed multiparametric fluorescence-activated cell sorting (FACS) analyses of circulating T and B lymphocytes (fig. S1, B to E) and measured antibodies induced against the SARS-CoV-2 nucleocapsid (N) and S proteins in patients' sera.

Among T lymphocytes, $CD8^+$ cells from patients with severe disease showed a reduced frequency of effector memory cells ($CD45RO^+$ and $CCR7^-$) and a decreased IFN-γ production capacity,

during the infection (Fig. 1C and figs. S1, B and C, and S2), paralleled by an increased relative abundance of naïve cells. The same alterations were observed for $CD4^+$ T cells, although less pronounced (figs. S1, B and D, and S2, B and C). The phenotyping of T helper (T_H) cells indicated a moderate increase in the frequency of nonconventional T_H1 (T_H1^*) cells in individuals with mild symptoms during the infection, which was reduced in patients with severe disease instead (figs. S1D and S2D). After the resolution of the infection, all patients with COVID-19 showed a significant impairment of the T_H1 subset. In patients with severe disease, the frequency of regulatory T (T_{reg}) cells was moderately reduced during the infection and that of T_H17 was increased post-infection, whereas the same subsets did not show any significant alteration in patients with mild disease (figs. S1D and S2D).

Within the B cell population, total memory B cells were more abundant in individuals with mild disease during the infection. This difference was magnified when looking at switched memory B cells and specifically at immunoglobulin M–positive (IgM^+) B lymphocytes, whereas the frequency of immunoglobulin G–positive (IgG^+) B cells did not significantly differ between patients. However, the relative abundance of the switched memory B cells, and of the IgG^+ ones in particular, was higher in severe patients post-infection. The frequency of plasmablasts was variable, with an increase that tended to be transient in mild patients and smaller but sustained in those with severe disease (Fig. 1D and fig. S1E).

We measured the anti–SARS-CoV-2 antibody plasma levels by enzyme-linked immunosorbent assay (ELISA), assessing IgM, IgA, and IgG polyclonal binding to the N protein and to the N-terminal S1, the receptor binding domain (RBD), and the C-terminal S2 domains of the S protein. N and RBD elicited the highest antibody titers. RBD stimulated a rather homogeneous antibody response in all patients with COVID-19, whereas S1 and S2 tended to be better recognized by antibodies from individuals with a severe disease (Fig. 1E). Overall, anti-N and anti-RBD IgG were detected during the infection and had the highest and comparable titers in all patients' groups. IgA were also detected against both proteins and tended to be higher in severe patients. IgM were more abundant in patients with severe disease, mainly recognizing RBD, whereas anti-N IgM was almost undetectable (Fig. 1E).

To evaluate the presence of potentially protective antibodies, we tested the ability of plasma samples to block the binding of a recombinant RBD protein to a human embryonic kidney (HEK) 293T cell line stably expressing the human ACE2 (hACE2) receptor. Neutralization of binding was higher in severe patients compared with those with mild disease and increased in both patient groups upon resolution of infection (Fig. 1F). Sera with neutralizing activity had detectable antibodies against S and RBD proteins, but we could not observe a clear correlation between anti-S antibody titers from a specific class and neutralization. Together, these data indicate a broad rearrangement of the adaptive immune system over time, involving both T and B lymphocytes, that was more evident in patients with severe disease.

Pervasive, graded, and durable transcriptional changes in PBMCs of patients with COVID-19

To get deeper insights into the evolution of the immune response against SARS-CoV-2, we analyzed the transcriptional profile and the T cell receptor (TCR) and B cell receptor (BCR) repertoires at the single-cell resolution of PBMC from six patients with COVID-19, three mild and three severe, and two healthy controls. Four of the

Fig. 1. Phenotypic analyses identify immune signatures in patients with COVID-19 during disease evolution. PBMCs from HDs (n = 4), patients with mild symptoms during infection and post-infection (n = 4), and severe disease during infection (n = 7) and post-infection (n = 6) phases analyzed by multiparametric flow cytometry. (**A**) Frequency of monocytes, B lymphocytes, T lymphocytes, CD3+ CD56+ cells, and NK cells is shown as percentage of live total PBMCs. (**B**) Frequency of CD4+ and CD8+ T lymphocytes is represented as percentage of live total PBMCs. (**C**) Relative abundance of CD8+ naïve, central memory (CM), effector memory (EM), and effector memory CD45RA+ (EMRA) cells is shown as percentage of live total CD8+ T lymphocytes. (**D**) Frequency of naïve B cells, total memory, non-switched memory, switched memory, memory IgM+, memory IgG+, and plasmablasts is shown as percentage of live total B lymphocytes; for memory IgM+ and memory IgG+ from severe patients during infection and post-infection, n = 5. (**E**) IgM, IgG, and IgA titers to SARS-CoV-2 nucleo-protein (N), RBD, S subunit 1 (S1), and subunit 2 (S2) measured by ELISA in the plasma of HDs (n = 5), mild patients during infection (n = 4) and post-infection (n = 4) and severe patients during infection (n = 7) and post-infection (n = 6). (**F**) Neutralization of binding of recombinant RBD protein to a HEK293T cell line expressing hACE2 by sera of HDs (n = 4), mild patients during infection (n = 4) and post-infection (n = 4), and severe patients during infection (n = 7) and post-infection (n = 6). Positivity threshold: 50% of binding inhibition. (A to F) Data are represented as box and whiskers showing median, min to max, and individual values. Statistical analyses were performed using Mann-Whitney t test to compare ranks. *P < 0.05; **P < 0.01. In (E), asterisk(s) above individual boxes denote statistical significance compared with HDs, whereas specific comparisons are defined by square brackets colored according to the Ig isotype considered in the comparison.
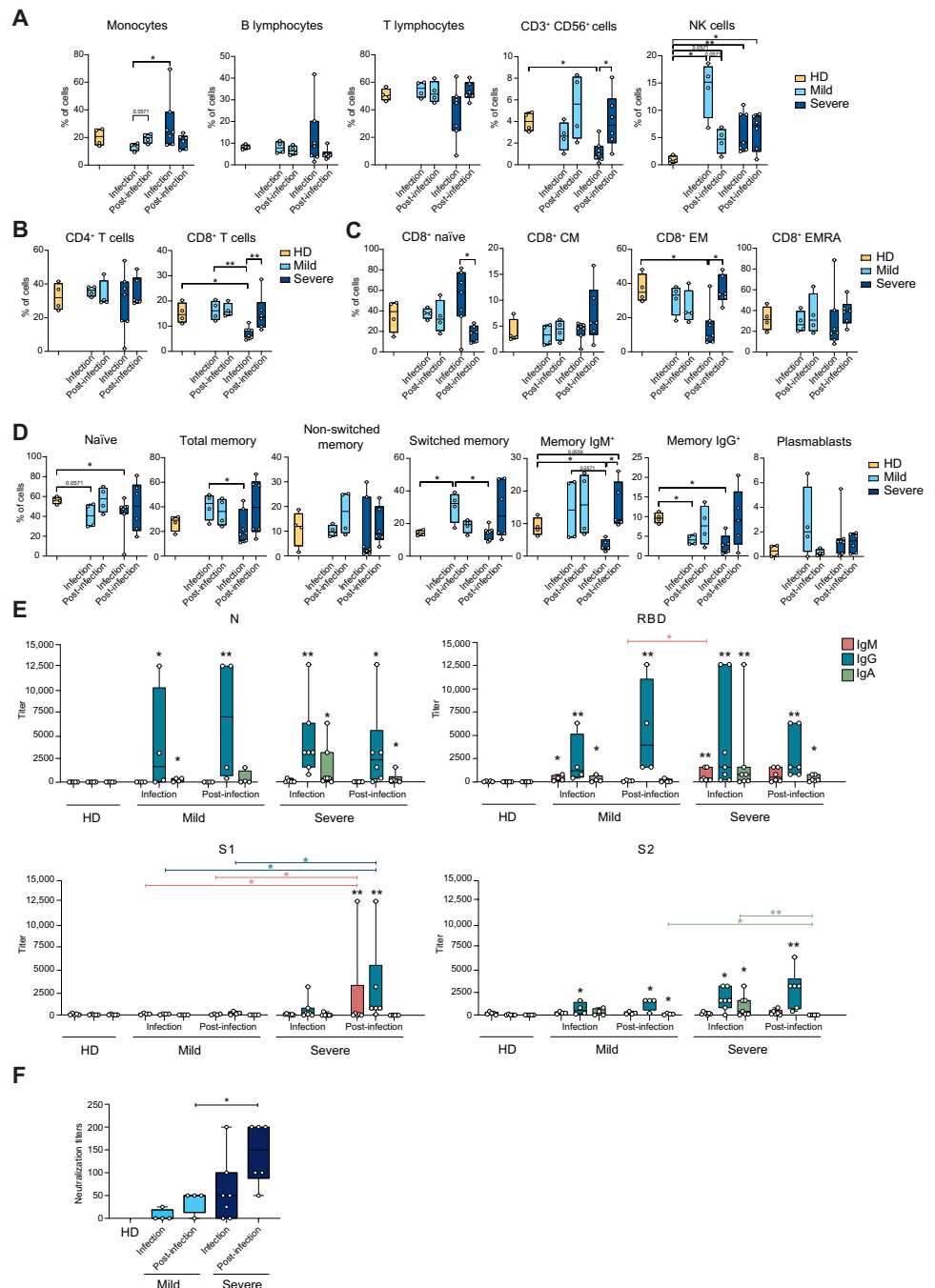
six patients with COVID-19, two mild and two severe, were profiled both during the infection (days 1 to 16 from diagnosis) and about 3 weeks after the infection resolution (days 19 to 21 from the negative swab, corresponding to days 50 and 51 from diagnosis), enabling us to dissect the development of the anti–SARS-CoV-2 immunity over the course of the disease.

Clustering of total PBMC single-cell RNA sequencing (scRNA-seq) profiles identified five distinct populations corresponding to the main circulating immune cell types: monocytes, NK cells, T and B lymphocytes, and megakaryocytes (Fig. 2A), defined by the combined expression of selected lineage-specific genes (fig. S3A).

The disease severity deeply influenced the transcriptome of all populations, resulting in a graded segregation of HDs from patients with mild and severe COVID-19 during the infection (fig. S3B, left). Such a pervasive effect was reduced post-infection, although the distribution of cells derived from patients was still clearly distinguishable from those of HDs (fig. S3B, right), indicating that the SARS-CoV-2 infection can affect the immunophenotype of exposed individuals for weeks after its resolution. Consistently with the literature (14–16), we observed a sizeable alteration of immune cells relative abundance in patients with COVID-19 compared with HDs both during the infection and post-infection (Fig. 2B). During
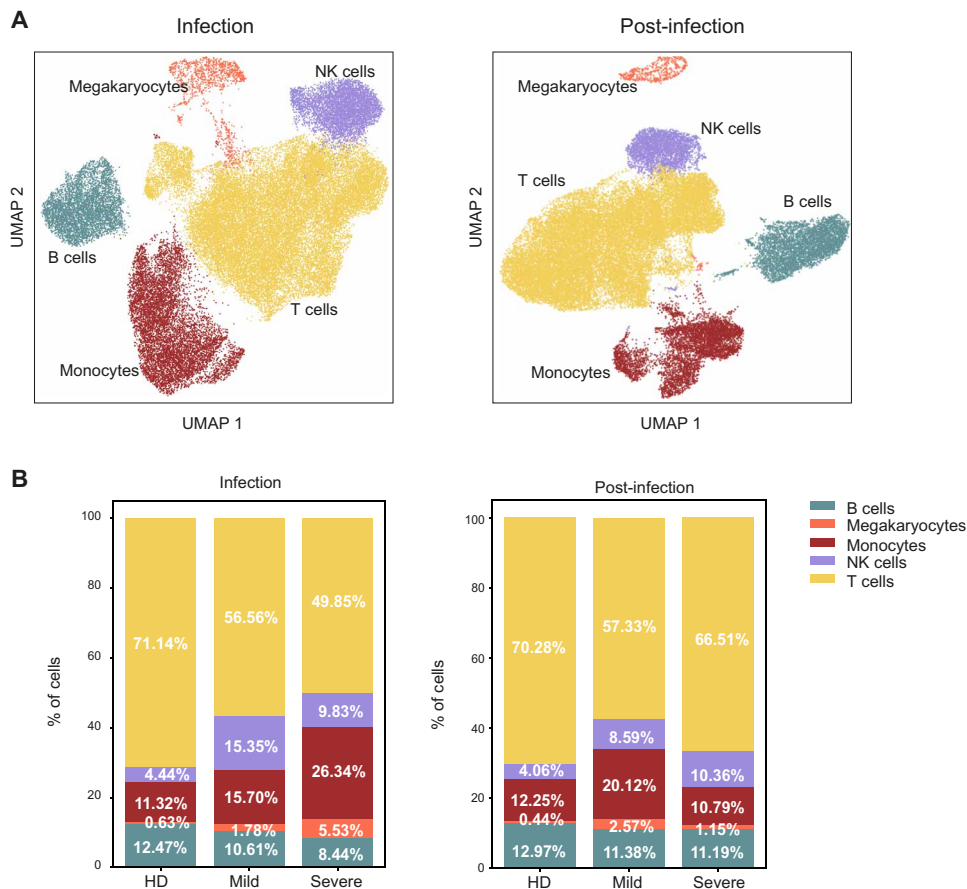
A

B

Fig. 2. Pervasive, graded, and durable transcriptional changes in the immune populations in patients with COVID-19. scRNA-seq of PBMCs from two HDs, three mild patients, and three severe patients. (**A**) UMAP identified immune cell populations during infection (left) and post-infection (right). (**B**) Barplots show the relative abundance of monocytes, NK cells, megakaryocytes, B lymphocytes, and T lymphocytes identified during infection (left) and post-infection (right). Percentages represent the average value of the patient cohorts.

COVID-19, sometimes with contrasting features (18–20). Therefore, we investigated the phenotype of circulating monocytes in our patients' cohort.

Transcriptional analysis identified seven monocyte clusters, one being largely populated by cells from HDs (Mo 5) (Fig. 3, A and B). During infection, monocytes from mild and severe patients were characterized by the prevalence of two clusters, Mo 1 and Mo 3, respectively (Fig. 3B and table S2). Differential expression and Gene Ontology analyses showed that cluster Mo 1 expressed high levels of human leukocyte antigen class II (HLA-II) genes, resembling monocytes differentiating into dendritic cells, whereas cluster Mo 3 was defined by the elevated expression of type I IFN–responsive genes (Fig. 3, C to E, and fig. S4, A and B). Patients with severe disease were also characterized by the lack of nonclassical monocytes (Mo 4), which have been associated with inflammation resolution (21) and which appeared after viral clearance (Fig. 3B). The post-infection phase was marked by the appearance of two additional clusters (Mo 6 and Mo 7), with cluster Mo 6 displaying activation (*FOS*, *JUN*, and *CD83*) and proinflammatory (*IL1B*, *CCL3*, *CCL4*, and *TNF*) features, more expanded in mild patients (Fig. 3, B and C).

These data indicate that monocytes from patients with severe COVID-19 showed an up-regulated type I IFN response signature compared with patients with mild disease and a considerable reduction of HLA-II genes expression (Fig. 3, D and E), a proposed surrogate marker of immunoparalysis in sepsis (22). The impaired HLA-II genes signature may result from the decreased IFN-γ production in severe patients (fig. S2B). Moreover, the appearance of a subpopulation expressing proinflammatory genes post-infection may underlie the persistence of an inflammatory status.

Distinct activation of "adaptive" and "inflamed" transcriptional programs in NK cells from patients with mild and severe COVID-19

NK cells are crucial in the defense against viral infections (23). We observed a significant increase in the frequency of NK cells in patients with mild disease during the infection compared with the other experimental groups, both by flow cytometry (Fig. 1A) and scRNA-seq (Fig. 2B). Thus, we determined whether NK cells from patients with mild and severe disease also had distinct expression profiles. Transcriptional analysis identified three major NK cell clusters (Fig. 3F): Clusters 0 and 1 were characterized by the low expression of *NCAM1* (CD56) paralleled by a high expression of *FCGR3A* (CD16) and several killer cell immunoglobulin-like receptors (KIRs) (fig. S4C), thus resembling CD56^{dim} CD16^{+} cytotoxic
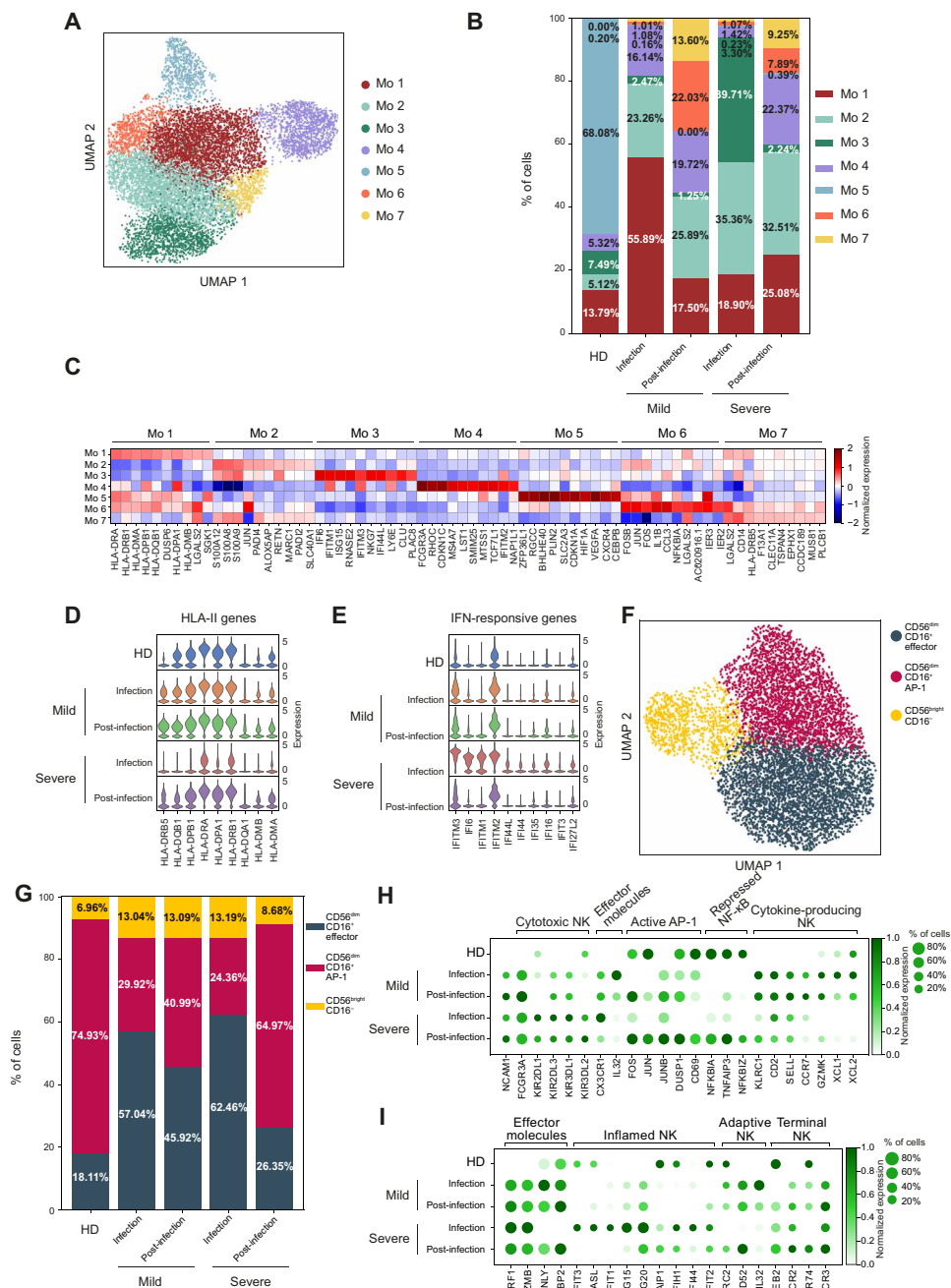
the infection, T lymphocytes showed reduced frequencies in patients, especially in those with severe disease. Conversely, monocytes and megakaryocytes showed a progressive increase from HDs to mild and severe COVID-19, whereas NK cells were especially expanded in patients with mild disease (Fig. 2B, left). After resolution of the infection, we observed a general trend toward the normalization of immune population abundance in severe patients, except for a residual expansion of NK cells (Fig. 2B, right). Mild patients retained an altered immune profile, with reduced T cell frequencies and an inflated innate immune compartment (monocytes, NK cells, and megakaryocytes) (Fig. 2B, right), suggesting a persistent inflammatory status.

Together, these transcriptomic data show that SARS-CoV-2 infection resulted in a long-lasting alteration of the circulating immune cell population composition. This effect was particularly evident during the acute immune response, when immune cells are recruited to the infected tissues, but persisted after the infection resolved.

Elevated type I IFN signaling and reduced HLA-II expression in monocytes from patients with COVID-19

Innate immune cells contribute to the systemic inflammation that characterizes severe COVID-19 (5, 17). The appearance of monocytes with an altered immune profile has been described in patients with

Fig. 3. Monocytes and NK cells phenotype in patient with COVID-19. (**A**) Monocytes from HDs and patients with COVID-19 were segregated into seven transcriptional clusters, visualized by UMAP. (**B**) Barplot illustrates the relative abundance of the seven subpopulations of monocytes in HDs and mild and severe patients during infection and post-infection. Percentages shown are the average of the indicated cohort, and individual values are reported in table S2. (**C**) Heatmap of the top 10 differentially expressed genes in the seven monocyte clusters. Violin plots show the expression of (**D**) HLA-II genes and (**E**) type I IFN–responsive genes in the indicated patient cohorts during and after infection. (**F**) NK cells from HDs and patients with COVID-19 were divided into three transcriptional clusters, visualized by UMAP. (**G**) Barplot illustrates the relative abundance of the three subpopulations of NK cells in HDs and patients with mild and severe disease during infection and post-infection. Percentages shown are the average of the indicated cohort, and individual values are reported in table S2. (**H** and **I**) Dotplots showing the expression of the indicated subset-specific genes in HDs and patients with mild and severe disease during infection and post-infection. NF-κB, nuclear factor κB.

NK cells (*24*). Clusters 0 and 1 showed limited differences that were mostly confined to an elevated expression of the effector molecules *CX3CR1* and *IL32* in cluster 0 (hereafter CD56^{dim} CD16$^+$ effector) and the activation of activator protein 1 (AP-1) and repression of nuclear factor κB pathways in cluster 1 (hereafter CD56^{dim} CD16$^+$ AP-1) (fig. S4C). On the contrary, cluster 2 had high expression of *NCAM1*, *KLRC1* (NKG2A), *CD2*, *CD62L*, and *CCR7* in the absence of *FCGR3A* and KIR transcription (fig. S4C), all features of CD56^{bright} CD16$^-$ cytokine-producing NK cells that secrete abundant cytokines and proliferate in response to cytokine stimulation but have limited cytotoxicity (*24*). The relative frequency of CD56^{dim} CD16$^+$ and CD56^{bright} CD16$^-$ NK cells was increased in patients with mild disease during and after infection and in patients with severe disease during the infection, whereas the proportion of the three NK subpopulations in individuals with severe disease post-infection was similar to the one observed in HDs (Fig. 3G and table S2).

Comparative transcriptional analysis showed that, during the infection, NK cells from mild patients expressed higher levels of genes typical of CD56^{bright} CD16$^-$ cytokine-producing cells, such as *KLRC1*, *GZMK*, *XCL1*, and *XCL2* (Fig. 3H). They also exhibited features of adaptive NK cells (*25*, *26*), such as the expression of *KLRC2*, *CD52*, and *IL32* (Fig. 3I). NK cells from severe patients upregulated instead the transcription of genes characteristic of CD56^{dim} CD16$^+$ effector cells, like *CX3CR1* and KIRs (Fig. 3H), but had an impaired expression of the activating receptor *KLRC2* (NKG2C) and of some cytotoxic molecules, such as *GNLY* and *FGFBP2* (Fig. 3I). NK cells from severe patients also expressed higher amounts of IFN-responsive genes, characteristic of inflamed NK cells (Fig. 3I) (*25*, *26*). Last, NK cells post-infection, especially from patients with severe disease, up-regulated the expression of *NCR3* (NKp30), *HAVCR2* [T-cell immunoglobulin and mucin-domain containing-3 (TIM-3)], and *WDR74*, that characterize terminally differentiated NK cells (Fig. 3I). These data indicate that, despite the similar subsets' frequency, NK cells from patients with mild and severe disease activated distinct transcriptional programs that may underlie a different capacity to control the viral infection.
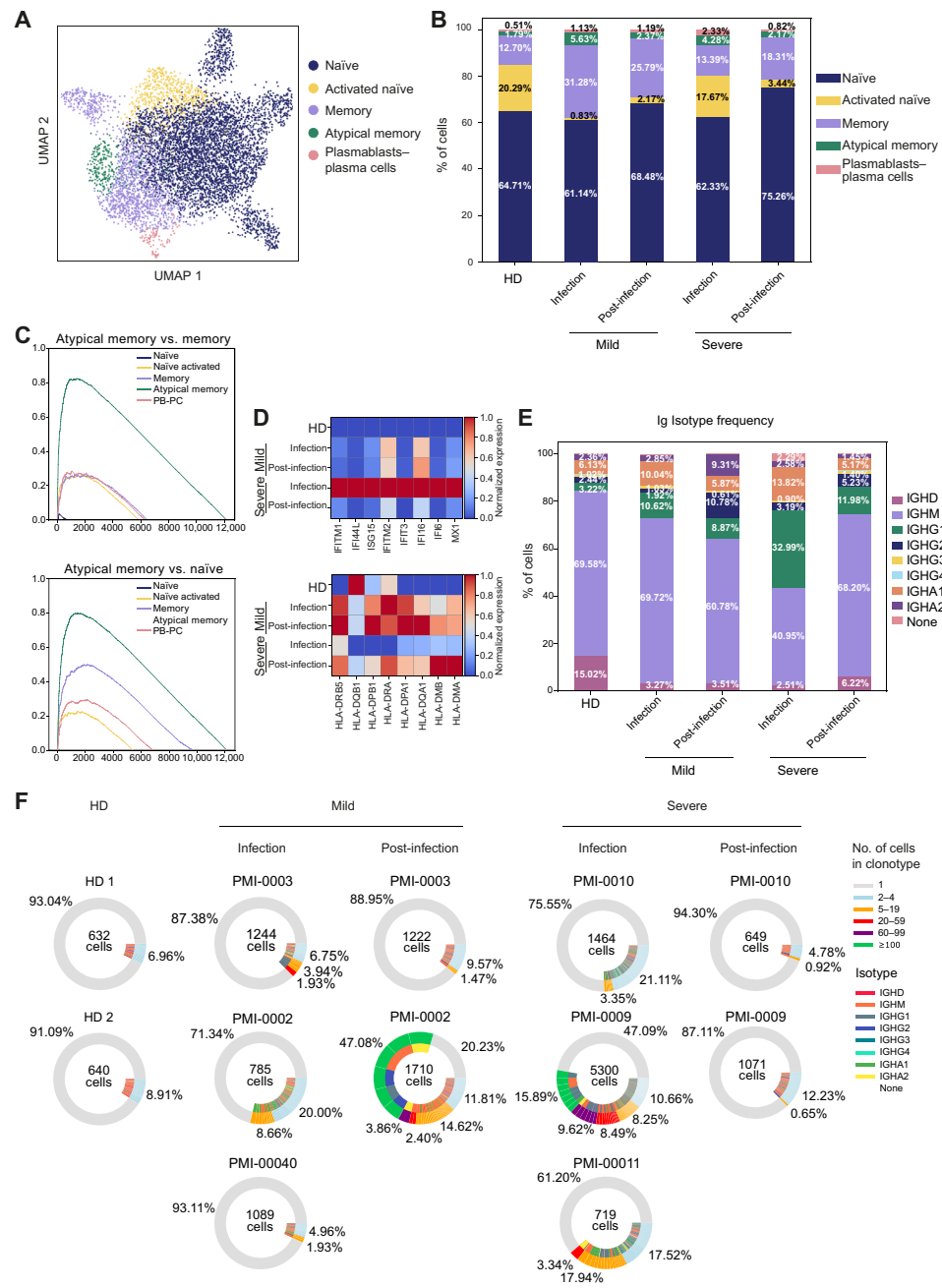
Fig. 4. Features of B cell subsets, immunoglobulin classes, and clonal expansion in patients with COVID-19. (**A**) UMAP depicting the six B cell clusters identified by transcriptional profiles. (**B**) Barplot showing the relative abundance of each B cell cluster in HDs and patients with mild and severe COVID-19 during and after infection. (**C**) GSEA showing the enrichment of the atypical memory B cells signature (table S4) in the identified B cell subsets. (**D**) Heatmap of type I IFN–responsive genes (top) and HLA-II genes (bottom) expression in B cells from HDs and mild and severe patients during infection and post-infection. (**E**) Immunoglobulin isotypes frequency in B cells from HDs and mild and severe patients during and after infection. (B and E) Percentages shown are the average of the indicated cohort; for individual values, refer to table S3. (**F**) Donut plots representing B cell clonal expansion (outer circle) and isotype usage (inner circle) in HDs and mild and severe patients during infection and post-infection. Each donut represents a single patient, and the number inside the donut is the number of cells analyzed.

Increased frequency of memory B cells in patients with COVID-19

Humoral immunity is key to neutralize viruses and to prevent reinfection. Thus, we explored the transcriptional phenotype of B

lymphocytes to identify peculiar populations induced by SARS-CoV-2 infection. Clustering of gene expression profiles revealed five different B cell subpopulations (Fig. 4A) that were annotated on the basis of the differential expression of selected markers (fig. S5A) as naïve (IGHD+ IGHM+), activated naïve (IGHD+ Nur77+), memory (CD27+), atypical memory (CD27+, CD21−, and FCRL5+), and plasmablasts/plasma cells (MZB1+ CD38+). The relative proportion of the major B cell subsets from scRNA-seq (Fig. 4B and table S3) was similar to that measured by flow cytometry (Fig. 1D). During the infection, patients with COVID-19 had an increased abundance of memory B lymphocytes, especially in individuals with mild disease (Fig. 4B). They were also characterized by the enrichment of a memory subset negative for *CR2* (CD21) transcription and expressing high levels of *FCRL5*, resembling an atypical memory B cell population described in other infectious diseases (*27, 28*) (Fig. 4B and fig. S5A). The identity of this population was confirmed by gene set enrichment analyses (GSEAs) (Fig. 4C and table S4). These cells up-regulated *CXCR3* and *TBX21* (T-bet) that is required for IgG2a class switching (*29, 30*), a feature important for clearing viral infections (*31*). During the infection, B cells from severe patients were characterized by the up-regulation of several type I IFN–responsive genes, paralleled by a partial down-regulation of major histocompatibility complex (MHC) II genes (Fig. 4D), as seen in monocytes.

Collectively, these analyses show an increased abundance of memory B lymphocytes in patients with COVID-19, especially in individuals with mild disease during the acute immune response, that were also characterized by the peculiar expansion of an atypical memory subpopulation. An elevated type I IFN response signature and the down-regulation of HLA-II genes expression were features of both monocytes and B cells from patients with severe COVID-19 during the infection, possibly indicating an impaired antigen presentation capacity.

Ig isotypes and B cell clonal expansion during and post-infection

To evaluate B cell class switching and clonal expansion, we performed single-cell BCR sequencing (BCR-seq) analysis. We measured the proportion of IgA, IgD, IgG, and IgM isotypes, whereas IgE was undetectable. IgM was the predominant immunoglobulin in all

samples, whereas IgG and IgA isotypes were more abundant in patients with COVID-19 compared with HDs. In particular, patients with severe disease showed the highest levels of IgG1 and IgA1 isotypes during the infection (Fig. 4E and table S3). The levels of IgG1 and IgA1 decreased post-infection, whereas IgG2 showed an opposite trend (Fig. 4E). Transcriptional profiles corroborated ELISA antibody measurement, revealing the preferential elicitation of IgA antibodies, especially against the RBD and N protein, in patients with severe disease (Fig. 1E).

Investigating the clonal expansion of circulating B cells, we observed a variegated response. During the infection, severe patients had a higher clonal expansion than mild patients, whereas post-infection we observed a generally reduced clonal expansion, with the exception of one of the two patients with mild disease (Fig. 4F). Expanded B cells included IgM, IgA2, and IgG subtypes. The B cell clones identified post-infection (fig. S5B), likely proliferating in response to SARS-CoV-2 antigens, did not match those captured during infection.

We also compared the preferential V(D)J gene usage in patients with COVID-19 and HDs. The IGHV3-23/IGHJ4 gene couple was enriched in all individuals, including HDs, whereas the IGHV4-34/IGHJ6 pair was specifically overrepresented in severe patients during the infection. An enrichment of several gene segments (IGHV3-48/J4, IGHV3-49/J4, IGHV4-28/J4, IGHV4-34/J6, IGHV4-39/J5, and IGHV5-51/J6) was found in patients with mild disease post-infection, instead. The overrepresentation of IGHV4-34/IGHJ6 genes in patients may indicate a specific rearrangement induced by SARS-CoV-2. We observed a similar pattern for light chains with the enrichment of a single gene pair (IGKV1-9/IGKJ3) in severe patients during the infection and of various combinations of gene segments in patients with mild disease post-infection (IGLV2-8/IGLJ2, IGLV2-14/IGLJ3, IGLV2-11/IGLJ1, IGKV1-5/IGKJ4, IGKV1D-33/IGKJ3, and IGKV1D-39/IGKJ2) (fig. S5, C and D). These results suggest a variable antibody response among patients with COVID-19, with increased frequencies of IgG2 and a broader Ig gene usage in patients with mild disease post-infection.

Altered composition of CD4$^+$ and CD8$^+$ T cell subsets in patients with COVID-19

Transient lymphopenia can characterize viral infections, can be induced by type I IFN response, and can occur before the peak in the T cell response (32, 33). Although all patients had less T lymphocytes during the infection (Fig. 2B, left), individuals with mild disease showed a relative expansion of the CD8$^+$ T cell population (Fig. 5A), indicating an ongoing CD8$^+$-mediated immune response, possibly relevant for the management of SARS-CoV-2 infection. On the contrary, patients with severe disease experienced a relative contraction of the CD8$^+$ lymphocytes compartment, resulting in an altered CD4/CD8 ratio (Fig. 5A).

Transcriptional analysis of T lymphocytes identified 11 clusters, including 6 CD4$^+$ and 5 CD8$^+$ lymphocyte subsets (Fig. 5B), annotated on the basis of inspection of selected marker genes (fig. S6A). CD4$^+$ T lymphocytes included T_H naïve, T_H central memory (T_{CM}), T_H2/T_H17, $T_H17/T_H1^*/T_H2$, $T_H1^*/T_H1/T_H17$, and T_{reg}; whereas CD8$^+$ lymphocytes were divided in cytotoxic T (T_C) naïve, T_C1 granzyme B$^+$ (GZMB$^+$), T_C1 granzyme K$^+$ (GZMK$^+$), and T_C17/mucosal-associated invariant T (MAIT) cells (Fig. 5B). CD8$^+$ lymphocytes also contained a cluster that was difficult to characterize on the basis of differentially expressed genes (dubbed as "uncharacterized") but likely largely populated by naïve and central memory (T_{CM}) cells from HDs (Fig. 5B). The heterogeneous expression of critical marker genes impeded to categorize these CD4$^+$ lymphocyte clusters as individual T_H subsets. However, we observed a phenotypic gradient reflecting the transition from central memory (T_H T_{CM} and T_H2/T_H17) to effector memory subsets ($T_H17/T_H1^*/T_H2$ and $T_H1^*/T_H1/T_H17$), highlighted by the progressive reduction in the expression of key genes leading to the recirculation to secondary lymphoid organs (CCR7 and SELL) (34, 35) and regulating self-renewal capacity (TCF7 and LEF1) (fig. S6A) (36).

Whereas the proportion of T_H naïve and T_{reg} cells did not vary across patient cohorts, we observed an increase in central memory subsets (T_{CM} and T_H2/T_H17) as disease severity progressed, especially during the infection (Fig. 5C and table S5). In particular, severe patients were characterized by the skewing toward a T_H2-like immune response and by the appearance of a T_{CM} cluster expressing the T follicular helper marker CXCR5 and IFN-responsive genes (Fig. 5, C and E, and fig. S6A).

Within the CD8$^+$ compartment, patients with COVID-19 displayed a relative expansion of T_C1 GZMB$^+$ cells during the infection that increased with disease severity, whereas the frequency of T_C1 GZMK$^+$ lymphocytes was highest in severe patients post-infection (Fig. 5D and table S5). These changes were confirmed at the protein level by flow cytometry where we observed a general increase in the frequency of GZMB$^+$ cells in patients with COVID-19 compared with HDs and of GZMK$^+$/GZMB$^+$ double-positive cells in patients with severe disease post-infection (Fig. 5F and fig. S1F). Both T_C1 subpopulations expressed genes coding for effector molecules, such as CCL5, NKG7, PRF1, GZMA, and CST7, although they were transcribed at higher levels in T_C1 GZMB$^+$ (fig. S6, A and C). The distinctive feature of the T_C1 GZMB$^+$ subset was an elevated production of GZMB, GNLY, and FGFBP2 accompanied by the expression of CD16 (FCGR3A) and several killer cell lectin receptors, like KLRD1, KLRF1, and KLRC3, normally expressed on NK cells, indicating that these cells may be highly cytotoxic (fig. S6, B, left, and C). Despite the expression of NK-related genes, T_C1 GZMB$^+$ cells displayed a variegated gene usage without a prevalence of the vα24-Jα18 genes in their TCR composition, indicating they were not invariant NKT (fig. S6D and table S6). T_C1 GZMK$^+$ cells were defined instead by the elevated expression of GZMK, CD160, and HLA-II genes (fig. S6B, right, and C). The elevated expression of HLA-DR and other HLA-II genes is associated with T cell activation and marks in vivo proliferating CD8$^+$ T lymphocytes with reduced cytolytic activity (37), although GZMK has been demonstrated to inhibit influenza virus replication (38). We explored the possibility that GZMB$^+$ cells were short-lived effector lymphocytes (SLECs), whereas GZMK-expressing cells represented MPECs (39, 40). T_C1 GZMB$^+$ lymphocytes expressed elevated CX3CR1, characteristic of highly differentiated effector cells (41), whereas T_C1 GZMK$^+$ cells expressed TCF7 (Fig. 5G), a feature of memory-like cells that are able to proliferate in chronic viral infections (42). Moreover, TCF-1 (the TCF7 gene product) expression is a feature of SARS-CoV-2–specific memory T cells isolated from convalescent individuals (43). To further support the idea that T_C1 GZMB$^+$ lymphocytes are SLECs and T_C1 GZMK$^+$ lymphocytes are MPECs, we performed GSEA comparing the expression profile of the CD8$^+$ subpopulations with the gene signatures of effector and memory human CD8$^+$ T lymphocytes generated in response to vaccination with the live attenuated yellow fever virus (YFV) (table S7) (44), one of the

Fig. 5. Altered composition of CD4+ and CD8+ T cell subsets in patients with COVID-19. (**A**) Barplot illustrates the percentages of CD4+ and CD8+ cells in CD3+ T lymphocytes of the patients analyzed. Percentages shown are the average of the cohort. (**B**) UMAP representing the 11 T cell clusters identified by transcriptional analysis. (**C**) Barplots describe the relative abundance of the identified CD4+ cell subsets in the cohorts analyzed during infection (left) and post-infection (right). (**D**) Barplots show the relative abundance of the identified CD8+ lymphocytes subpopulations in the cohorts analyzed during infection (left) and post-infection (right). (C and D) Percentages shown are the average of the indicated cohort, and individual values are reported in table S5. (**E**) Heatmap of type I IFN–responsive genes expression in the CD4+ T cell subsets. (**F**) Frequency of CD8+ GZMB+, CD8+ GZMK+, and CD8+ GZMB+/GZMK+ cells detected by multiparametric flow cytometry in PBMCs of HDs ($n = 4$), mild patients during ($n = 4$) and after ($n = 4$) infection, and severe patients during ($n = 7$) and after ($n = 6$) infection. Data represent the percentage of live total CD8+ T lymphocytes and are visualized as box and whiskers showing median, min to max, and individual values. (**G**) Dotplots showing the expression of *CX3CR1* (top) and *TCF7* (bottom) in the T_C1 GZMK+ and T_C1 GZMB+ clusters. (**H**) GSEA analysis showing enrichment of the human effector T cell signature in CD8+ clusters. (**I**) GSEA analyses showing enrichment of the human memory T cell signature (left) and human effector T cell signature (right) in the T_C1 GZMK+ and T_C1 GZMB+ clusters. Human effector and memory CD8+ T lymphocytes gene sets were derived from the analysis of the GSE100745 GEO Dataset (table S7). (**J**) GSEA analyses showing enrichment of terminal effectors KLRG1hi signature (left) and memory precursors KLRG1int signature (right) in the T_C1 GZMK+ and T_C1 GZMB+ clusters. Mouse KLRG1hi and KLRG1int gene sets were extracted from the Molecular Signature Database (GSE10239) (table S7). In (F), statistical analyses were performed using Mann-Whitney t test to compare ranks. *$P < 0.05$; **$P < 0.01$.
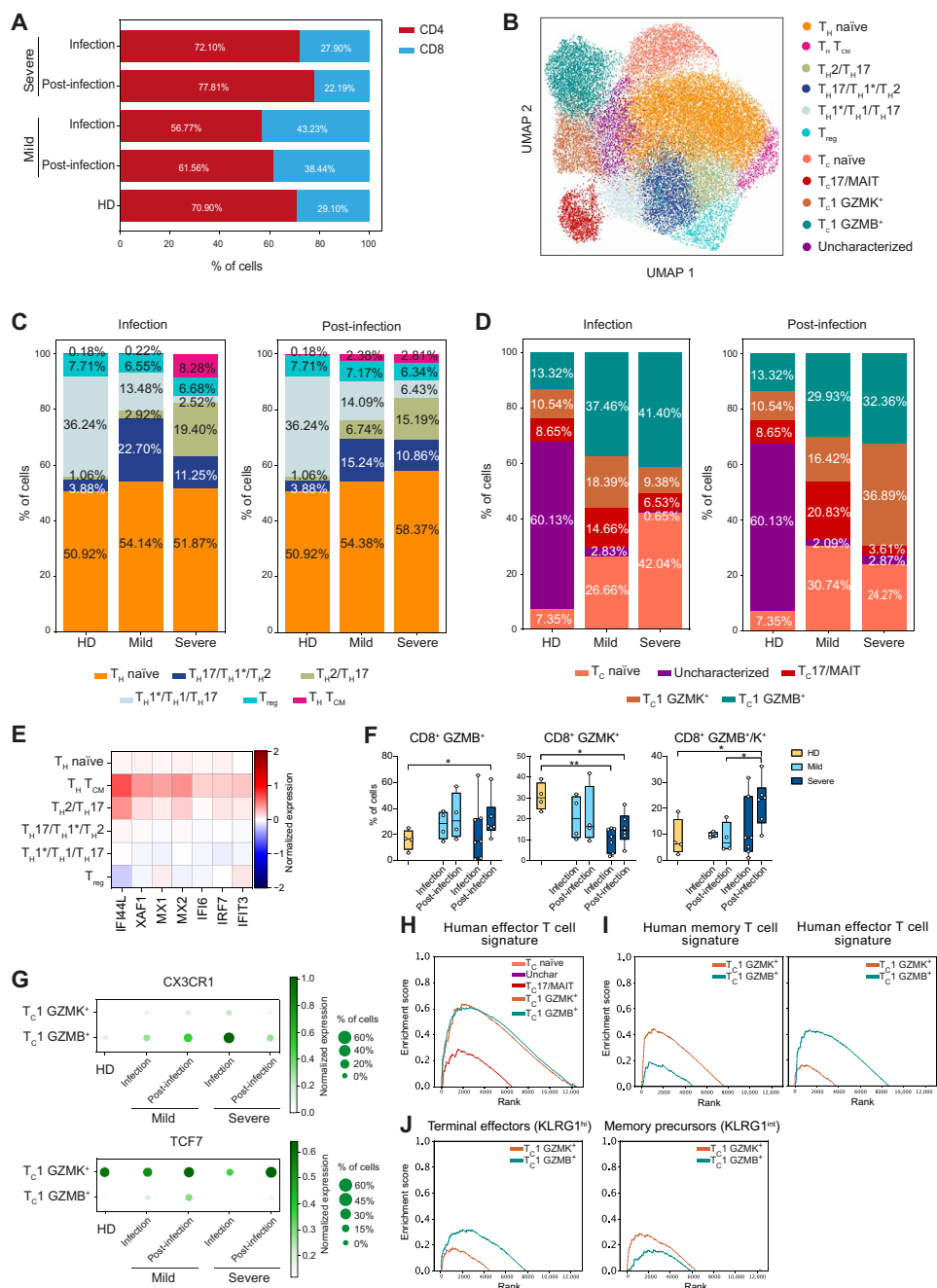
best-established models of acute viral infection in humans. Looking at the global transcriptional profile, both GZMB+ and GZMK+ cells showed a footprint of effector T lymphocytes (Fig. 5H), but focusing on the subset of differentially expressed genes, the GZMK+ cells were enriched for a signature of memory lymphocytes (Fig. 5I). In addition, when compared with the gene sets characterizing SLEC and MPEC defined by killer cell lectin like receptor G1 (KLRG1) expression in a mouse model of lymphocytic choriomeningitis virus acute infection (table S7) (*45*), the GZMB+ cells showed a relative enrichment in the transcriptional profile of KLRG1hi terminal effectors, whereas GZMK+ cells in that of KLRG1int memory precursors (Fig. 5J).

Patients with mild disease had a higher frequency of T_C17-like cells than severe patients (Fig. 5D). This subset was defined by the

expression of *KLRB1* (CD161), *SLC4A10*, *RORC*, and *CCR6* (fig. S6, A and C), and the TCR gene usage (*TRAV1-2*, *TRAJ33/12/20*, and *TRBV20/6*) demonstrated that these were primarily composed of MAIT cells (fig. S6F and table S6) (*46*, *47*). Similar to T_C1 GZMK+ cells, MAIT cells displayed a moderate expression of effector molecule–coding genes, such as *CCL5*, *NKG7*, *PRF1*, *CST7*, and *GZMK* (fig. S6, A to C), the latter being a feature of MAIT cells TCR-independent activation, resulting in a slower response with limited inflammation (*48*). MAIT cells showed an increased expression of the activation markers *CD69*, *FOS*, and *DUSP1* in patients with mild COVID-19 and the up-regulation of IFN-responsive genes in patients with severe disease, during the infection (fig. S6G).

Collectively, these data indicated a T_{CM}- and T_H2-skewed $CD4^+$ T cell response in patients with severe disease accompanied by a type I IFN–responsive gene signature. $CD8^+$ lymphocytes from patients with COVID-19 were characterized by an elevated frequency of terminally differentiated $GZMB^+$ effector cells during the infection, followed post-infection by an increased abundance of $GZMK^+$ effector cells that may represent memory cell precursors.

CD4$^+$ and CD8$^+$ T cell clonal expansion in patients with COVID-19

To better dissect the SARS-CoV-2–specific T cell immune response, we speculated that expanded T cell clonotypes represented lymphocytes proliferating upon antigenic stimulation in response to SARS-CoV-2 infection, possibly accompanied by some bystander activation. To support the assumption, we generated antigen-specific, primary $CD4^+$ T cell populations against SARS-CoV-2 RBD, S1, and N proteins and verified the appearance of expanded clonotypes identified by single-cell TCR sequencing (scTCR-seq) analysis within these polyclonal populations. We detected the TCR-β of four of six clonotypes tested (Fig. 6A), providing evidence that a sizeable proportion of the expanded T lymphocytes identified by single-cell sequencing analyses is specific for SARS-CoV-2. Thus, we focused on the phenotypic characterization of the expanded T cell clones as a proxy for the SARS-CoV-2–specific T lymphocytes. We observed a higher clonal expansion for $CD8^+$ T lymphocytes in patients with COVID-19 compared with HDs, although the absolute number of expanded cells was substantially lower in severe patients during the infection (Fig. 6B and table S8). On the contrary, $CD4^+$ T lymphocytes showed a limited clonal expansion even post-infection (Fig. 6C, fig. S7, A and B, and table S8). Although the clonal expansion was distributed in all non-naïve $CD8^+$ subsets, it was mostly confined to the $T_H1^*/T_H1/T_H17$ subpopulation in T_H cells (fig. S7, A and B, and table S9). However, the phenotype of expanded $CD4^+$ T lymphocytes changed according to the disease severity: It was dominated by $T_H1^*/T_H1/T_H17$- and $T_H17/T_H1^*/T_H2$-like cells in mild patients and by T_H2/T_H17 and T_{CM} cells in patients with severe
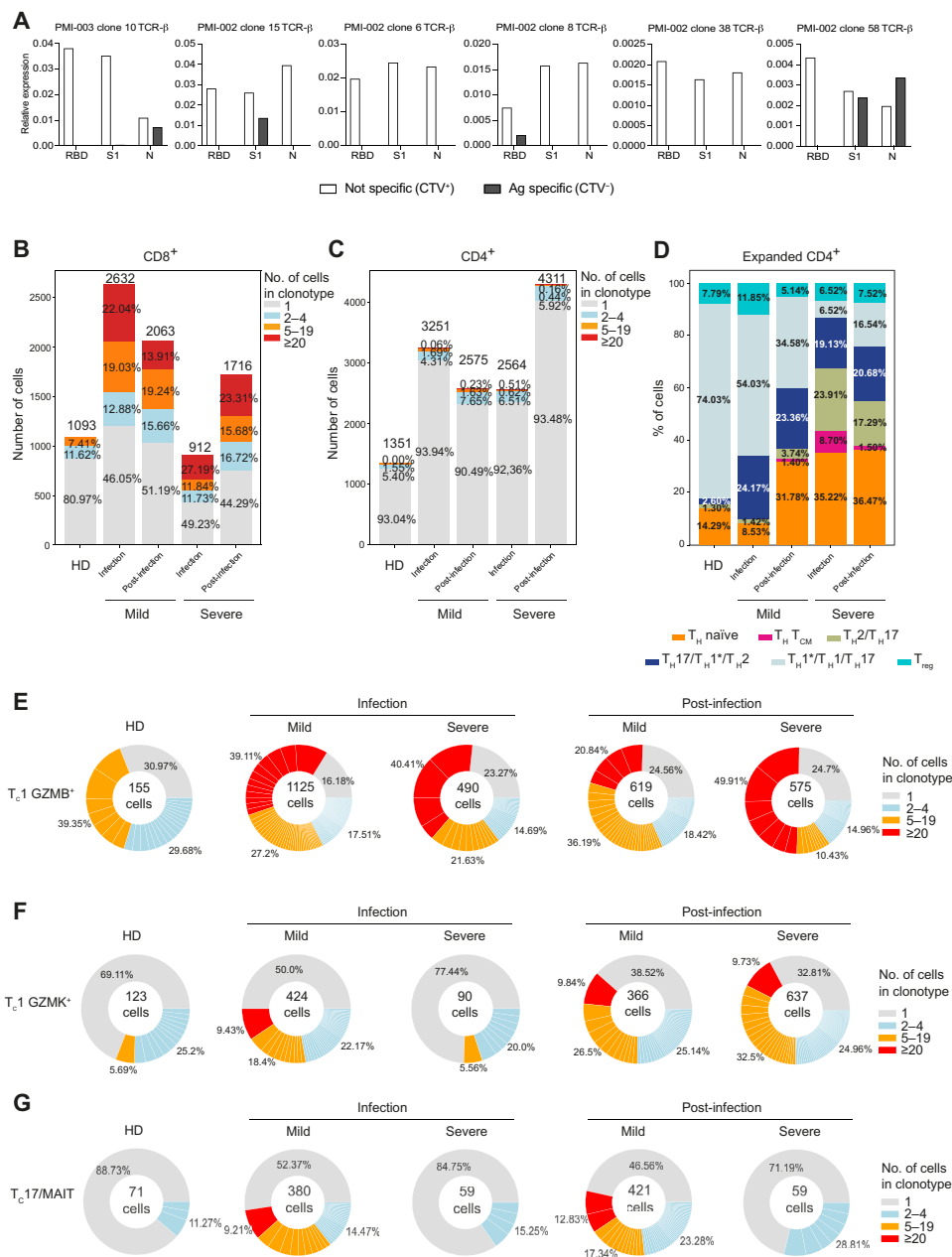

Fig. 6. CD4$^+$ and CD8$^+$ T cell clonal expansion in patients with COVID-19. (**A**) Primary $CD4^+$ T cell populations specific to SARS-CoV-2 RBD, S1, and N proteins were generated from two patients with mild disease post-infection, and the presence of TCR-β chains of selected expanded clonotypes identified by scRNA-seq was detected by TCR-targeted SMART–quantitative PCR assay. Barplots show $CD8^+$ (**B**) and $CD4^+$ (**C**) T cell clonal expansion in HDs and mild and severe patients during and after infection. Numbers above the bars represent the total number of cells in the mentioned cohorts, and values inside the bars represent the percentage of cells in each group of clonal expansion; percentages represent the average of the cohort, and individual values are detailed in table S8. (**D**) Barplots show the relative abundance of the expanded $CD4^+$ T lymphocytes in HDs and mild and severe patients during and after infection. Percentages shown are the average of the indicated cohort, and individual values are reported in table S9. Donut charts describe the clonal expansion in T_C1 $GZMB^+$ (**E**), T_C1 $GZMK^+$ (**F**), and $T_C17/MAIT$ (**G**) populations in the indicated patient cohorts and time points. The total number of cells in the population inside the donut and the mean percentage for each clonal expansion group are represented; individual values for each patient are detailed in table S9.

disease (Fig. 6D and table S9). In addition, the expanded $CD4^+$ T lymphocytes showed an enhanced expression of effector molecules in mild patients, whereas those from patients with severe disease

expressed higher amounts of proapoptotic genes, as well as *SOCS1* and *SOCS3* (fig. S7C) that dampen the calcium signaling downstream the TCR (*49*) and inhibit the signal transducer and activator of transcription (STAT) pathway activation (*50*).

Among the CD8$^+$ T cell subsets, T_C1 GZMB$^+$ cells were expanded in patients with COVID-19 both during the infection and post-infection (Fig. 6E and table S9), whereas T_C1 GZMK$^+$ lymphocytes showed an enhanced clonal expansion after the infection resolution (Fig. 6F and table S9). Both T_C1 GZMB$^+$ and T_C1 GZMK$^+$ expanded clonotypes expressed high *KLRG1* (fig. S7D), a marker of effector T cells (*51*). In addition, expanded T_C1 GZMB$^+$ expressed *TBX21* (T-bet) and lost the expression of *CD27* and *CD28*, and a small fraction of them up-regulated *HAVCR2* (TIM-3) (fig. S7, D and E). Instead, expanded T_C1 GZMK$^+$ expressed *CD27*, whose interaction with CD70 on antigen-presenting cells (APCs) promotes the generation and maintenance of memory cells (*52*), *EOMES*, *TCF7*, and very low *CX3CR1* levels (fig. S7D), resembling mouse effector T lymphocytes transitioning to memory precursors (*53*). Only a small fraction of expanded T_C1 GZMB$^+$ and T_C1 GZMK$^+$ cells expressed coinhibitory receptors (fig. S7E), suggesting that they were not exhausted T lymphocytes. A small proportion of expanded T_C1 GZMK$^+$ cells also expressed *CXCR5* and *BCL6* (fig. S7D), a feature of follicular cytotoxic CD8$^+$ T lymphocytes, which can contribute to the control of chronic viral infections (*54*, *55*).

Last, T_C17/MAIT cells were exclusively expanded in patients with mild symptoms, both during the infection and post-infection (Fig. 6G and table S9). The same trend of clonal proliferation was shown in the two patients that could be analyzed during the infection only (fig. S7F). The patient with severe symptoms who completely lacked a CD8$^+$ lymphocyte clonal expansion, suggesting that he failed to mount an effective cytotoxic immune response, succumbed to the disease, similarly to what has been recently reported (*13*).

Together, these data demonstrate that SARS-CoV-2 infection elicited a vigorous cytotoxic T cell immune response accompanied by a limited proliferation of T helper lymphocytes. The CD8$^+$ response was dominated by the proliferation of GZMB$^+$ cells throughout the infection, whereas GZMK$^+$ cells were particularly expanded after the infection resolution and had several transcriptional features associated to memory precursors.

Maintenance of highly expanded CD8$^+$ clonotypes with focused plasticity within granzyme-producing subsets

To explore the clonal relationship between the different T cell subpopulations, we monitored the evolution of the expanded clonotypes, grouped according to their phenotype, in each patient from the infection to the post-infection phase. Only the highly expanded clonotypes were retained throughout the course of the immune response (Fig. 7, A and B; fig. S8, A and B; and table S10). Thus, only a minority of CD4$^+$ lymphocytes were found both during the infection and post-infection, namely, 37 of 211 clonotypes (17.54%) corresponding to 139 of 510 cells (27.25%). The few expanded clones were largely confined to the $T_H1^*/T_H1/T_H17$ subset (fig. S8, A and B) with limited plasticity toward phenotypically related populations, such as the $T_H17/T_H1^*/T_H2$ subset (fig. S8C). Similarly, among the CD8$^+$ T lymphocytes, the most expanded clonotypes were those retained after the resolution of infection, but their higher clonal expansion resulted in the sharing of 118 of 162 clonotypes (72.84%), corresponding to 2213 of 2533 cells (87.34%). To substantiate this finding, we analyzed CD8$^+$ T lymphocytes isolated

10 months after the infection from two of the patients with mild disease. Only a small fraction (12.55 and 16.64%) of the clonotypes not expanded during the infection was detected at this time point, whereas most of the expanded clonotypes persisted, with an increased frequency of lymphocytes derived from the T_C1 GZMK$^+$ subset (fig. S8D). Most of the proliferating clones during and post-infection were T_C1 GZMB$^+$ cells, but they showed a relatively high plasticity toward the T_C1 GZMK$^+$ subset (Fig. 7C), supporting the idea that the two populations may represent different developmental stages in the immune response rather that two functionally distinct clusters. Instead, MAIT cells constituted a clonally independent CD8$^+$ subpopulation (Fig. 7C), as expected because of their restricted TCR gene usage.

To highlight the relationship between the two granzyme-producing subsets, we performed RNA velocity analysis (*56*). CD8$^+$ T lymphocytes from patients with COVID-19 showed an increased length of the velocity vectors compared with those from HDs (fig. S9A), indicating an ongoing alteration of the cell state. The RNA velocity was higher for the effector subsets and reduced post-infection (fig. S9A), suggesting a trend toward a partial restoration of quiescence after the pathogen clearance. CD4$^+$ T lymphocytes showed a similar picture (fig. S9B). A subset of T_C1 GZMB$^+$ cells was predicted to transdifferentiate into T_C1 GZMK$^+$ cells (Fig. 7D), further supporting a developmental trajectory where a fraction of short-lived effectors fuels the generation of memory precursors.

To reveal whether evolutive pressures acted on the selection of expanded clonotypes preserved after infection resolution, we compared the complementarity-determining regions (CDR1, CDR2, and CDR3) aminoacidic sequences of expanded clonotypes during the infection and post-infection. Although we identified only a "public" clonotype among two mild patients, defined as a complete CDR1, CDR2, and CDR3 homology, we observed a small enrichment of a limited set of CDR1 and CDR2 in the TCR of expanded lymphocytes post-infection (Fig. 8).

Collectively, these data demonstrated that only highly proliferating clonotypes were maintained after resolution of infection, part of which probably forming a pool of SARS-CoV-2–specific memory cells. A proportion of the CD8$^+$ expanded clonotypes were found both in the T_C1 GZMB$^+$ and in the T_C1 GZMK$^+$ subsets indicating a common ancestry. Last, TCR composition analysis of the expanded clonotypes that were retained post-infection revealed a diversity in their repertoire accompanied by the selection of a small set of common CDRs, suggesting the presence of some physical constraint needed for the recognition of cognate antigens.

DISCUSSION

Knowledge on the temporal evolution of the immune response in patients with COVID-19 is especially valuable in interpreting SARS-CoV-2 adaptive immunity and for the optimization of effective vaccines. In this study, we integrated single-cell phenotypic and repertoire analyses to investigate the immune response in patients with COVID-19 with mild and severe symptoms during the acute disease and after the resolution of the infection. The collected data describe the development of immune responses in these patients, suggesting a prominent role for CD8$^+$ T lymphocytes in clearing SARS-CoV-2 infection.

We confirmed that SARS-CoV-2 infection results in a profound remodeling of the circulating immune cell populations, especially in
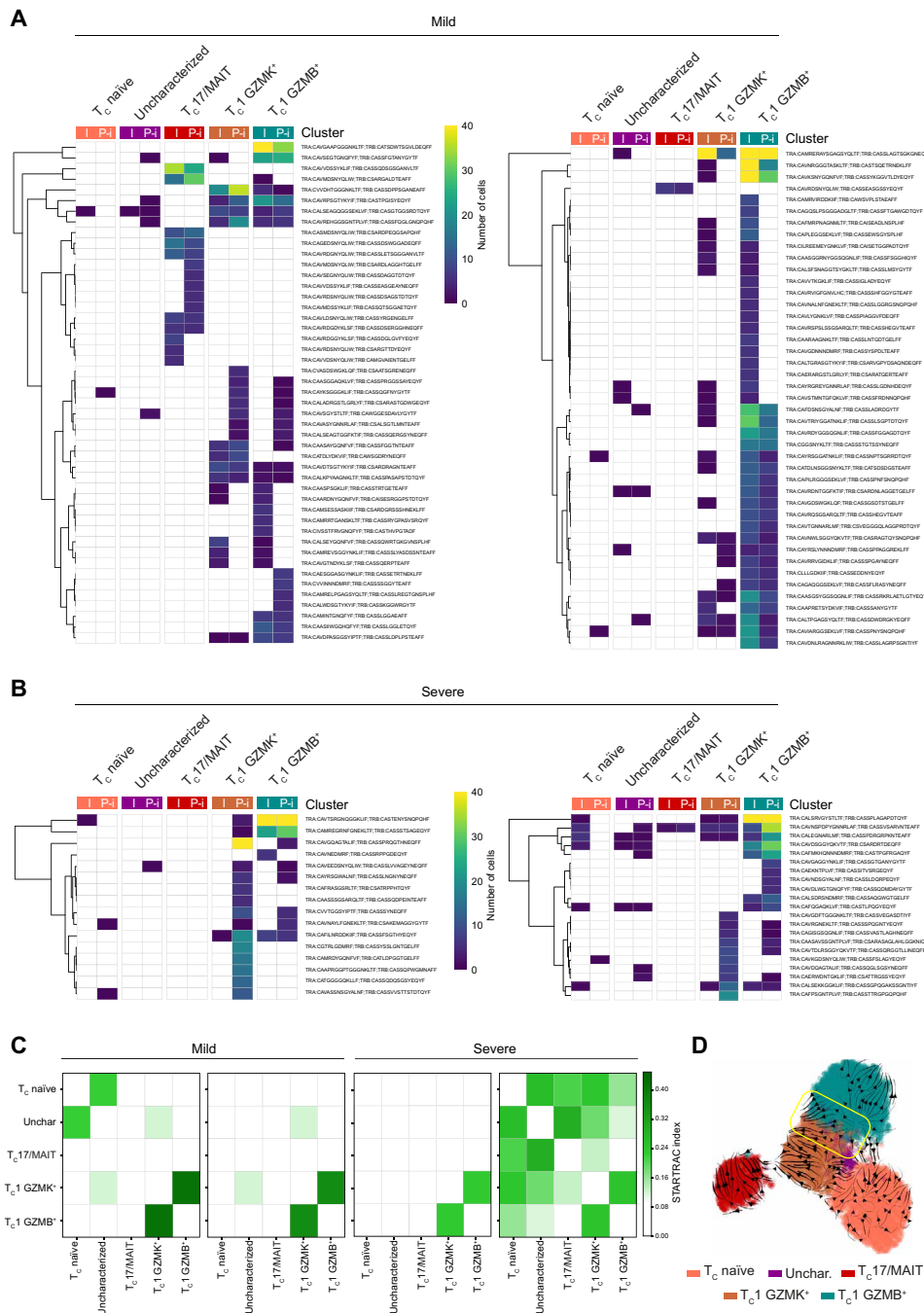
Fig. 7. Highly expanded CD8^{+} clonotypes persist post-infection and show focused plasticity within granzyme-producing subsets. Heatmaps demonstrate clonotype sharing between CD8^{+} T cell clusters from infection (I) to post-infection (P-i) phases in mild (**A**) and severe (**B**) patients with COVID-19. TCR-α (TRA) and TCR-β (TRB) CDR3 sequences are listed in table S10. (**C**) STARTRAC transition index describes the degree of clonotype sharing and plasticity among the different CD8^{+} T cell clusters in the two mild and two severe patients analyzed. (**D**) RNA velocity vectors plotted on a UMAP representing CD8^{+} T lymphocytes from patients with COVID-19. The yellow box highlights a subset of T$_C$1 GZMB[+] cells predicted to transdifferentiate into T$_C$1 GZMK^{+} cells.

new insight on the post–COVID-19 syndrome (*59*). We observed that the extensive transcriptional alteration was characterized by a pervasive type I IFN response signature that crossed all the immune populations, especially involving monocytes. Type I IFN signaling has a prominent role in the innate immune response against viruses, and its impairment or temporal dysregulation associates with severe COVID-19 (*11, 60, 61*). Some studies highlight that type I IFN signaling is lower in COVID-19 compared with other respiratory viral infections (*19, 62*). Although the intensity of the IFN response is higher in individuals with severe disease compared with those with mild symptoms (*18*) and correlates with the viral load (*62*), the opposite scenario is observed in critically ill patients (*63*). We identified an up-regulated type I IFN–responsive gene signature in patients with severe disease compared with individuals with mild symptoms, paralleled by an impaired antigen presentation transcriptional program and the lack of nonclassical monocytes, other prominent features of patients with severe COVID-19 (*5, 20, 64, 65*).

NK cells are crucial in the defense against viral infections because they kill infected cells and bridge the gap between the innate immune response and the setting of an optimal adaptive immunity. We found an increased frequency of NK cells in patients with mild disease during the infection, including both CD56^{dim} CD16^{+} effector and CD56^{bright} CD16^{−} cytokine-producing and adaptive NK cells, which have been originally identified in human cytomegalovirus infections and can form a pool of memory-like cells (*24*). On the contrary, NK cells from patients with severe disease showed an impaired production of cytotoxic molecules during the infection and were skewed toward an inflamed phenotype, whose impact on their antiviral activity will require additional investigation.

Pathogen-specific antibodies are fundamental to provide protection against virus reinfection. The magnitude of antibody response correlates with viral load and disease severity (*66*). Coherently, our data showed that the amount of neutralizing antibodies increased with disease severity and was higher post-infection. Although, the neutralization titers in severe patients did not perfectly match the kinetics of the antibody response against RBD, suggesting that
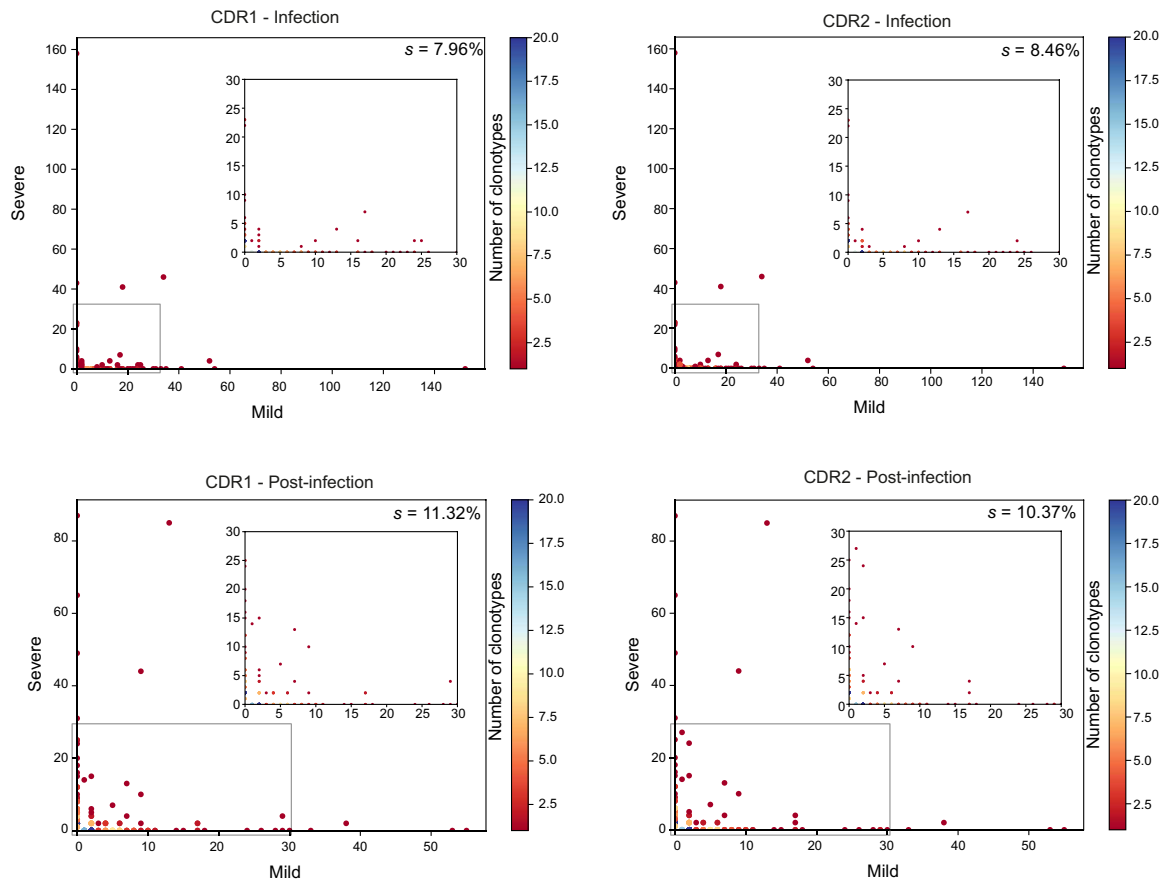
patients with a severe disease (*12, 57, 58*). The immune remodeling is echoed by pervasive, graded, and durable changes at the transcriptional level (*15, 17*) that lasted weeks after the infection resolution. A deeper understanding of this long-lasting perturbation may provide

Fig. 8. Expanded clonotypes retained post-infection are private but share a small set of CDR1 and CDR2. Sharing of CDR1 (left panels) and CDR2 (right panels) from the expanded clonotypes of four patients with COVID-19, two mild and two severe, during infection (top panels) and after infection (bottom panels). The percentage of shared regions (*s*) is shown. Overlapping clonotypes are colored as indicated in the heatmap. In each panel, the inset is a zoom-in of the area highlighted by the gray rectangle.

antibodies directed to other S domains may contribute to neutralize the binding of RBD to the host cells. Our data confirmed that the N and RBD proteins represent immunodominant antigens eliciting the highest IgG titers (*13, 67, 68*). Although the antibody response was dominated by IgG, we also detected IgA primarily in patients with severe disease, which could contribute to the tissue damage in severe COVID-19 (*69*). The IgM response was also higher in patients with severe disease, mostly directed against the RBD, and persisted post-infection, suggesting that these patients might have experienced a delayed elicitation of the antibody response.

Along with an overall increase of memory B cells in patients with COVID-19, we found the expansion of an atypical memory subpopulation during the infection (*70, 71*). Atypical memory B lymphocytes are thought to be functionally impaired, but recent evidence suggests that they are instead mature and optimally responsive cells (*72, 73*). In addition, their elevated T-bet expression may underlie an activation state and suggest that they can mount a T cell–independent immune response (*30, 74*). This feature, together with the ability to induce IgG2a class switching (*75*), may contribute to improved antiviral protection because viruses can act as T cell–independent antigens in vivo (*76*).

As for monocytes, we observed in B cells the up-regulation of various type I IFN–responsive genes, specifically in patients with

severe disease during the infection (*14, 19, 20*). Moreover, the down-regulation of HLA-II genes expression in these cells indicated that SARS-CoV-2 infection can impair the antigen presentation capacity of different kind of APCs. Last, analysis of B cell repertoire revealed that expanded B cell clones detected during the infection were distinct from those retrieved post-infection. A prolonged patients' monitoring would be needed to correlate the presence of expanded clonotypes with the acquisition of humoral immunity.

T lymphocytes are pivotal in tackling viral infections and establishing a protective immunological memory because cytotoxic CD8^{+} T lymphocytes kill infected cells and CD4^{+} T helper cells provide the signals to optimize effective and durable adaptive immune responses (*77, 78*). T cells underwent an extensive remodeling in patients with COVID-19 both in terms of abundance and phenotype. We found that T helper lymphocytes from individuals with mild disease were enriched in T_H17- and T_H1^*-like cells. T helper lymphocytes were partially skewed, instead, toward a T_{CM} and T_H2-like phenotype in patients with severe disease. The same trend was maintained and even enhanced when focusing on the expanded clonotypes that were enriched in SARS-CoV-2–specific T cells. An enhanced type 2 immune response is seen in fatal SARS-CoV infections (*79*) and severe COVID-19 cases (*11, 80*) and has detrimental effects in other respiratory infections (*81*). During the infection, CD4^{+} T lymphocytes

from severe patients also displayed the appearance of a T_{CM}-like subset characterized by a type I IFN response signature. Among the genes up-regulated in this signature, the X-linked inhibitor of apoptosis–associated factor 1 gene (*XAF1*) triggers apoptosis under stress conditions (*82*) and can induce increased T lymphocyte apoptosis in patients with COVID-19 (*18*), suggesting that an impaired T cell survival may represent one of the factors leading to lymphopenia in patients with severe disease. In addition, we found that expanded CD4$^+$ T lymphocytes from patients with severe disease expressed higher amounts of proapoptotic genes and lower levels of effector molecules, indicating an impaired fitness and a possible defect in mounting an effective antiviral response.

CD8$^+$ T lymphocytes have the largest contraction in absolute numbers in patients with COVID-19 during infection (*12, 15, 83*). Despite this, we observed a relative increase in the frequency of non-naïve T lymphocytes in patients compared with HDs. These cells could be distinguished in GZMB$^+$, GZMK$^+$, and MAIT cells. The different proportions of CD8$^+$ T lymphocytes in patients with mild and severe COVID-19 may suggest qualitative or temporal differences in the cell-mediated immune response depending on disease severity.

The longitudinal integrated analyses of transcriptomes and TCR repertoires in patients with COVID-19 coupled with immunophenotyping allowed us to depict the evolution of T cell responses in SARS-CoV-2–infected individuals by comparing and contrasting the phenotype of clonally expanded T lymphocytes as a proxy for antigen-specific cells. Here, we show that the expanded clonotypes detected by scTCR-seq included some SARS-CoV-2–specific T cells. We observed an enhanced CD8$^+$ T lymphocyte clonal expansion in patients with COVID-19 compared with HDs, indicating an ongoing adaptive cellular response in patients, although it was curbed in individuals with severe disease. The CD8$^+$ T cell clonal expansion was paralleled by less evident CD4$^+$ T lymphocytes clonal expansion, similarly to what is described in other acute viral infections (*84*). Among CD8$^+$ T lymphocytes, we found that GZMB$^+$ effector cells, expressing high levels of cytotoxic molecules, were considerably expanded during the infection and post-infection in all patients with COVID-19, regardless of disease severity. On the contrary, GZMK$^+$ lymphocytes, which showed several features of memory-like cells and had lower expression of effector molecules, were preferentially expanded post-infection and were retained in higher proportions months after the clearance of the pathogen, likely representing MPECs. The appearance of MPECs may be indicative of a resolution of the viral infection, because a curtailed antigenic stimulation during the later stages of infection enhances the generation of memory cells, whereas the continuous exposure to antigenic stimuli drives the differentiation of terminal effectors (*45*). Thus, the appearance of expanded T_C1 GZMK$^+$ lymphocytes might represent a prognostic factor of COVID-19 resolution. Another interesting observation was the presence of expanded MAIT cells specifically in mild patients. Although these cells are primarily characterized for their capacity to specifically recognize bacterial and fungal metabolites presented by the MHC class I–like molecule MR1 (*85*), they have antiviral capacity in response to bystander activation (*86*). Whether MAIT cells can restrain SARS-CoV-2 replication and which factors modulate their frequencies in patients with COVID-19 require further investigation.

In conclusion, our data demonstrated that activation of cytotoxic T lymphocytes marked natural immune response against SARS-CoV-2. In line with the evidence that coordinated T and B cell immune responses positively correlated with COVID-19 prognosis (*13*), a variety of effective vaccines against SARS-CoV-2 have been developed that elicit antigen-specific CD4$^+$ and CD8$^+$ T lymphocytes and SARS-CoV-2–neutralizing antibodies. The extent of the duration of the protective immunity to SARS-CoV-2 induced by infection and vaccines is a subject of ongoing discussion. SARS-CoV–specific memory T lymphocytes last many years after infection (*9, 87*), and SARS-CoV-2–specific memory T and B cells persist for months after the infection (*88–91*), hinting at long-term immunity. The detection of antigen-specific MPECs may represent an early-stage correlate of durable memory. The limited clonal expansion that we observed for CD4$^+$ T lymphocytes was in contrast to that of CD8$^+$ T lymphocytes, but in line with that observed in virus-naïve individuals in other models of acute viral infections, like the YFV vaccination. YFV recall vaccination induces higher expansion of antigen-specific CD4$^+$ T cells compared with the first challenge (*84*). It will be interesting to verify whether anti–SARS-CoV-2 vaccines will be able to boost a similar T helper clonal expansion to elicit a long-lasting protective immunity and to compare the immunological memory induced by natural infections and vaccines.

Collectively, this study describes the development of an adaptive immune response in individuals who had mild or severe COVID-19. It provides insights into the generation of a T cell–driven immune response to SARS-CoV-2, by delineating the features of an effector GZMK$^+$ CD8$^+$ T lymphocyte population that may generate protective memory against SARS-CoV-2.

MATERIALS AND METHODS

More details on all of these techniques can be found in the Supplementary Materials.

Study design
The objective of the study was to describe the immune response to SARS-CoV-2 infection in patients with different grades of COVID-19 disease severity. Serological, phenotypic, and transcriptomic analyses were combined to describe features associated with SARS-CoV-2 infection. We investigated innate and adaptive immune responses in 17 patients, with mild ($n = 6$) or severe ($n = 11$) disease, during and after infection, and compared with healthy individuals ($n = 5$).

Sample collection
Patients enrolled in the study were diagnosed on the basis of a reverse transcription polymerase chain reaction (PCR)–positive nasopharyngeal swab for SARS-CoV-2. They were classified as affected by severe disease (radiological diagnosis of pneumonia and/or respiratory failure, i.e., pO$_2$ < 80 mmHg or pCO$_2$ < 35 mmHg or satO$_2$ < 94% in ambient air) or by mild disease (no symptoms or fever >37.5°C, cough, or coryza, without evidence of pneumonia and/or respiratory failure). The study was approved by the Institutional Review Board Milano Area 2 (#331_2020).

PBMC isolation
In brief, PBMCs were isolated by density-gradient centrifugation following the Ficoll-Paque Plus standard protocol.

FACS immunophenotyping
In brief, 100,000 cells were washed in phosphate-buffered saline (PBS) 1×, stained with Fixable Viability Stain 15 min at room temperature

(RT), and then washed in magnetic-activated cell sorting (MACS) buffer. For the detection of cell surface proteins, cells were stained with the indicated antibodies diluted in Brilliant Stain Buffer solution (1:2 in MACS buffer) for 30 min at RT. After washing in MACS buffer, cells were fixed 15 min at 4°C using the eBioscience FOXP3 staining kit and washed again in MACS buffer before acquisition. For intracellular cytokine staining, cells were stimulated for 4 hours with 0.2 μM phorbol 12-myristate 13-acetate and ionomycin (1 μg/ml) in culture medium at 37°C. Brefeldin A (10 μg/ml) was added in the last 2 hours of stimulation. To detect intracellular proteins, cells were permeabilized and stained in Permeabilization Reagent supplemented with antibodies for 30 min at 4°C. All incubation steps were performed in the dark. Antibodies used for FACS are listed in table S11.

Expression and purification of SARS-CoV-2 proteins
In brief, on the basis of an early SARS-CoV-2 sequence isolate (Wuhan-Hu-1), human codon-optimized nucleotide sequences encoding the subunits of the S glycoprotein, S1 (amino acids 2 to 673), S2 (amino acids 686 to 1211), and RBD (amino acids 318 to 541), and the full-length N protein, were synthesized and cloned into a pcDNA 3.4 vector. Recombinant proteins included a custom N-terminal signal peptide for protein secretion and a C-terminal octa-histidine tag for purification. Plasmids were transiently transfected into Expi293 cells, and after 72 hours, recombinant proteins were purified from culture supernatants by immobilized metal affinity chromatography.

Enzyme-linked immunosorbent assay
Anti-S1, anti-S2, anti-RBD, and anti-N IgG, IgM, and IgA plasma titers were determined by ELISA. In brief, 96-well plates were coated overnight at 4°C with 250 ng per well of each recombinant protein in PBS 1×. After blocking with PBS/bovine serum albumin (BSA) 5%, plasma samples were serially diluted and incubated for 1 hour at 37°C. Plates were washed with PBS/Tween 0.5% and probed with horseradish peroxidase–conjugated α-human IgG, IgM, and IgA secondary antibodies (1:1000 in PBS/BSA 1%/Tween 0.5%) for 40 min RT. After washing, the reaction was developed with 3,3′,5,5′-tetramethylbenzidine (TMB) for 10 min and stopped with 100 μl of 1 M H_2SO_4, and the absorbance was measured at λ = 450 nm.

Neutralization of binding assay (NOB)
In brief, to evaluate the concentration of serum neutralizing antibodies, 10 μl of purified recombinant RBD–Alexa Fluor 647 [10 μg/ml in PBS/fetal calf serum (FCS) 1%] were mixed with 10 μl of different sera dilutions in U-bottom 96-well plates for 1 hour at RT. After incubation, 30×10^3 HEK293TN-hACE2 cells were resuspended in 5 μl of PBS/FCS 1%, added to the mix, and incubated 1 hour at 4°C. Unbound protein was removed by washing with PBS, and RBD binding was detected by flow cytometry. Specific binding neutralization was calculated as follows: NOB (%) = 1 − (MFI$_{Sample}$ − MFI$_{background}$)/(MFI$_{CtrlNegative}$ − MFI$_{background}$).

Generation of hACE2 cell line
In brief, a cell line stably expressing hACE2 receptor (HEK293TN-hACE2) was generated by lentiviral transduction of HEK293TN cells with pLENTI_hACE2_HygR, obtained by hACE2 subcloning from pcDNA3.1-hACE2 into pLenti-CMV-GFP-Hygro, and now available to the scientific community through Addgene (no. 155296). Lentiviral particles were produced by calcium phosphate–based cotransfection of third-generation helper and transfer plasmids, following standard procedures. Forty-eight hours after transduction, HEK293TN were subjected to hygromycin selection. Expression of hACE2 was confirmed by flow cytometry.

Generation of antigen-specific primary CD4+ T cells
Briefly, to generate SARS-CoV-2–specific polyclonal T cell populations, monocytes from patients' total PBMCs were isolated with human CD14 microbeads, irradiated (45 Gy), and loaded with the recombinant S1, RBD, and N proteins, by incubating 1×10^5 cells with antigen (4 μg/ml) in complete medium for 6 hours. Loaded monocytes were then coincubated with sorted and Cell Trace Violet (CTV)–stained total memory CD4+ T cells at 1:2 ratio in complete medium in flat-bottom 96-well plates. On day 3, cells were resuspended and transferred to U-bottom 96-well plates. On day 6, CTV− were sorted and expanded with allogeneic irradiated feeder cells and phytohemagglutinin (1 μg/ml) in complete medium containing IL-2 (500 U/ml).

TCR-targeted SMART–quantitative PCR
Briefly, to identify the presence of individual T cell clonotypes in the polyclonal SARS-CoV-2–specific T cell populations, a method was set up on the basis of a modified SMART-seq2 protocol.

Single-cell RNA sequencing
PBMCs were thawed in culture medium. Viability was measured immediately before chip loading, exceeding 75% in all samples. Ten thousand PBMCs per sample were loaded on a Chromium 10X Controller to generate single-cell Gel Beads in Emulsion (GEMs), according to the Chromium Next GEM Single Cell 5′ Library and Gel Bead Kit v1.1 protocol. Gene expression, TCR, and BCR enriched libraries were produced using the Chromium Single Cell 5′ Library Construction Kit according to the manufacturer's instructions. Indexed libraries were sequenced on an Illumina NovaSeq Flow-Cell Type S2 (2× 150–base pair paired-end).

scRNA-seq data processing and quality control
Raw fastQ files were aligned against the GRCh38 human reference genome and quantified using Cell Ranger Single-Cell 10X pipeline with default parameters. The filtered cell barcode matrices of each sample obtained by Cell Ranger count were processed using Scanpy (v1.4.2). Samples were grouped on the basis of the stage of the disease (infection versus post-infection). To identify cell populations, we performed separated analyses on the two stages. The different batches were aggregated with concatenate function with basic quality control (QC) filtering. For each sample, cells that expressed <200 genes and genes detected in less than 0.1% of the total cells were filtered out. A second filter was applied to remove low-quality cells on the basis of the median absolute deviation obtained from the distribution of the number of expressed genes per cell, Unique Molecular Identifier (UMI) counts, and the percentage of mitochondrial and riboprotein genes. The obtained dataset was then normalized and log-transformed using Scanpy pp.normalize_per_cell and pp.log1p functions, and technical sources of variation were regressed out by pp.regress_out. For the subsequent analyses, a set of high variable genes was identified with pp.highly_variable_genes (mean expression ranging from 0.0125 and 5 and dispersion greater than 0.01).

Dimensionality reduction and clustering
Briefly, principal components analysis (tl.pca function) was used to identify significant principal components in the dataset. Selection of

the number of components for the nearest-neighbor network computation (pp.neighbors) was based on their visualization in an elbow plot (pl.pca_variance_ratio). Uniform manifold approximation and projection (UMAP) was performed for the spatial visualization of the single-cell dataset and features. Last, cells were clustered using the Leiden algorithm.

Differential expression analyses

Differentially expressed genes between the distinct clusters and experimental groups were identified with the tl.rank_genes_groups function and filtered on the basis of adjusted P value (≤ 0.05) and $\log_2$ fold change (≥ 1). Gene Ontology analyses on differentially expressed genes were performed using Metascape with GO Biological Processes as Pathway and default parameters.

RNA velocity

RNA velocity analysis was performed using the scvelo python package (v.0.2.3), applying a dynamical model. The number of spliced and unspliced reads was counted directly on the Cell Ranger output, and the calculated RNA velocity vectors were embedded in a UMAP space. Velocities were estimated by inferring the splicing kinetics of the top 50 differentially expressed genes in each population.

TCR-seq and BCR-seq

Raw fastQ files were assembled using the Cell Ranger VDJ 10X pipeline with default parameters to obtain CDR3 sequences and the rearrangement of V(D)J genes. For TCRs, only cells with a productive TCR-α and TCR-β chains pair and for BCRs only those with at least a productive heavy and light chains pair were considered for further analyses. A clonotype was defined by consistent CDR3 amino acid sequence and V and J gene usage. Cells sharing the same clonotype were considered clonal, and the clonotype as clonally expanded.

STARTRAC transition index

For clonally expanded CD4$^+$ (clonotypes ≥ 2 cells) and CD8$^+$ (clonotypes ≥ 5 cells) T cells, STARTRAC transition index for each batch was calculated as described (92). Plot and figures were generated using seaborn 0.10.1 and matplotlib 3.3.1.

Statistics

Statistical analyses of flow cytometry and serological data were performed with GraphPad Prism software. Statistical significance between groups was determined using Mann-Whitney test to compare ranks. P values ≤ 0.05 were considered significant.

SUPPLEMENTARY MATERIALS

immunology.sciencemag.org/cgi/content/full/6/62/eabg5021/DC1
Extended Materials and Methods
Figs. S1 to S9
Tables S1 to S11
Data file S1
View/request a protocol for this paper from *Bio-protocol*.

REFERENCES AND NOTES

1. G. Grasselli, A. Zangrillo, A. Zanella, M. Antonelli, L. Cabrini, A. Castelli, D. Cereda, A. Coluccello, G. Foti, R. Fumagalli, G. Iotti, N. Latronico, L. Lorini, S. Merler, G. Natalini, A. Piatti, M. V. Ranieri, A. M. Scandroglio, E. Storti, M. Cecconi, A. Pesenti; COVID-19 Lombardy ICU Network, Baseline characteristics and outcomes of 1591 patients infected with SARS-CoV-2 admitted to ICUs of the Lombardy Region, Italy. *JAMA* **323**, 1574–1581 (2020).

2. S. Richardson, J. S. Hirsch, M. Narasimhan, J. M. Crawford, T. McGinn, K. W. Davidson; Northwell COVID-19 Research Consortium, Presenting characteristics, comorbidities, and outcomes among 5700 patients hospitalized with COVID-19 in the New York City area. *JAMA* **323**, 2052–2059 (2020).

3. A. B. Docherty, E. M. Harrison, C. A. Green, H. E. Hardwick, R. Pius, L. Norman, K. A. Holden, J. M. Read, F. Dondelinger, G. Carson, L. Merson, J. Lee, D. Plotkin, L. Sigfrid, S. Halpin, C. Jackson, C. Gamble, P. W. Horby, J. S. Nguyen-Van-Tam, A. Ho, C. D. Russell, J. Dunning, P. J. Openshaw, J. K. Baillie, M. G. Semple; ISARIC4C investigators, Features of 20 133 UK patients in hospital with covid-19 using the ISARIC WHO Clinical Characterisation Protocol: Prospective observational cohort study. *BMJ* **369**, m1985 (2020).

4. G. Chen, D. Wu, W. Guo, Y. Cao, D. Huang, H. Wang, T. Wang, X. Zhang, H. Chen, H. Yu, X. Zhang, M. Zhang, S. Wu, J. Song, T. Chen, M. Han, S. Li, X. Luo, J. Zhao, Q. Ning, Clinical and immunological features of severe and moderate coronavirus disease 2019. *J. Clin. Invest.* **130**, 2620–2629 (2020).

5. A. Silvin, N. Chapuis, G. Dunsmore, A. G. Goubet, A. Dubuisson, L. Derosa, C. Almire, C. Henon, O. Kosmider, N. Droin, P. Rameau, C. Catelain, A. Alfaro, C. Dussiau, C. Friedrich, E. Sourdeau, N. Marin, T. A. Szwebel, D. Cantin, L. Mouthon, D. Borderie, M. Deloger, D. Bredel, S. Mouraud, D. Drubay, M. Andrieu, A. S. Lhonneur, V. Saada, A. Stoclin, C. Willekens, F. Pommeret, F. Griscelli, L. G. Ng, Z. Zhang, P. Bost, I. Amit, F. Barlesi, A. Marabelle, F. Pene, B. Gachot, F. Andre, L. Zitvogel, F. Ginhoux, M. Fontenay, E. Solary, Elevated calprotectin and abnormal myeloid cell subsets discriminate severe from mild COVID-19. *Cell* **182**, 1401–1418.e18 (2020).

6. A. Grifoni, D. Weiskopf, S. I. Ramirez, J. Mateus, J. M. Dan, C. R. Moderbacher, S. A. Rawlings, A. Sutherland, L. Premkumar, R. S. Jadi, D. Marrama, A. M. de Silva, A. Frazier, A. F. Carlin, J. A. Greenbaum, B. Peters, F. Krammer, D. M. Smith, S. Crotty, A. Sette, Targets of T cell responses to SARS-CoV-2 Coronavirus in humans with COVID-19 disease and unexposed individuals. *Cell* **181**, 1489–1501.e15 (2020).

7. J. Braun, L. Loyal, M. Frentsch, D. Wendisch, P. Georg, F. Kurth, S. Hippenstiel, M. Dingeldey, B. Kruse, F. Fauchere, E. Baysal, M. Mangold, L. Henze, R. Lauster, M. A. Mall, K. Beyer, J. Rohmel, S. Voigt, J. Schmitz, S. Miltenyi, I. Demuth, M. A. Muller, A. Hocke, M. Witzenrath, N. Suttorp, F. Kern, U. Reimer, H. Wenschuh, C. Drosten, V. M. Corman, C. Giesecke-Thiel, L. E. Sander, A. Thiel, SARS-CoV-2-reactive T cells in healthy donors and patients with COVID-19. *Nature* **587**, 270–274 (2020).

8. L. Ni, F. Ye, M. L. Cheng, Y. Feng, Y. Q. Deng, H. Zhao, P. Wei, J. Ge, M. Gou, X. Li, L. Sun, T. Cao, P. Wang, C. Zhou, R. Zhang, P. Liang, H. Guo, X. Wang, C. F. Qin, F. Chen, C. Dong, Detection of SARS-CoV-2-specific humoral and cellular immunity in COVID-19 convalescent individuals. *Immunity* **52**, 971–977.e3 (2020).

9. N. Le Bert, A. T. Tan, K. Kunasegaran, C. Y. L. Tham, M. Hafezi, A. Chia, M. H. Y. Chng, M. Lin, N. Tan, M. Linster, W. N. Chia, M. I. Chen, L.-F. Wang, E. E. Ooi, S. Kalimuddin, P. A. Tambyah, J. G. Low, Y.-J. Tan, A. Bertoletti, SARS-CoV-2-specific T cell immunity in cases of COVID-19 and SARS, and uninfected controls. *Nature* **584**, 457–462 (2020).

10. Y. Peng, A. J. Mentzer, G. Liu, X. Yao, Z. Yin, D. Dong, W. Dejnirattisai, T. Rostron, P. Supasa, C. Liu, C. Lopez-Camacho, J. Slon-Campos, Y. Zhao, D. I. Stuart, G. C. Paesen, J. M. Grimes, A. A. Antson, O. W. Bayfield, D. Hawkins, D. S. Ker, B. Wang, L. Turtle, K. Subramaniam, P. Thomson, P. Zhang, C. Dold, J. Ratcliff, P. Simmonds, T. de Silva, P. Sopp, D. Wellington, U. Rajapaksa, Y. L. Chen, M. Salio, G. Napolitani, W. Paes, P. Borrow, B. M. Kessler, J. W. Fry, N. F. Schwabe, M. G. Semple, J. K. Baillie, S. C. Moore, P. J. M. Openshaw, M. A. Ansari, S. Dunachie, E. Barnes, J. Frater, G. Kerr, P. Goulder, T. Lockett, R. Levin, Y. Zhang, R. Jing, L. P. Ho; Oxford Immunology Network Covid-19 Response T cell Consortium; ISARIC4C Investigators, R. J. Cornall, C. P. Conlon, P. Klenerman, G. R. Screaton, J. Mongkolsapaya, A. McMichael, J. C. Knight, G. Ogg, T. Dong, Broad and strong memory CD4$^+$ and CD8$^+$ T cells induced by SARS-CoV-2 in UK convalescent individuals following COVID-19. *Nat. Immunol.* **21**, 1336–1345 (2020).

11. C. Lucas, P. Wong, J. Klein, T. B. R. Castro, J. Silva, M. Sundaram, M. K. Ellingson, T. Mao, J. E. Oh, B. Israelow, T. Takahashi, M. Tokuyama, P. Lu, A. Venkataraman, A. Park, S. Mohanty, H. Wang, A. L. Wyllie, C. B. F. Vogels, R. Earnest, S. Lapidus, I. M. Ott, A. J. Moore, M. C. Muenker, J. B. Fournier, M. Campbell, C. D. Odio, A. Casanovas-Massana, I. T. Yale, R. Herbst, A. C. Shaw, R. Medzhitov, W. L. Schulz, N. D. Grubaugh, C. Dela Cruz, S. Farhadian, A. I. Ko, S. B. Omer, A. Iwasaki, Longitudinal analyses reveal immunological misfiring in severe COVID-19. *Nature* **584**, 463–469 (2020).

12. D. Mathew, J. R. Giles, A. E. Baxter, D. A. Oldridge, A. R. Greenplate, J. E. Wu, C. Alanio, L. Kuri-Cervantes, M. B. Pampena, K. D'Andrea, S. Manne, Z. Chen, Y. J. Huang, J. P. Reilly, A. R. Weisman, C. A. G. Ittner, O. Kuthuru, J. Dougherty, K. Nzingha, N. Han, J. Kim, A. Pattekar, E. C. Goodwin, E. M. Anderson, M. E. Weirick, S. Gouma, C. P. Arevalo, M. J. Bolton, F. Chen, S. F. Lacey, H. Ramage, S. Cherry, S. E. Hensley, S. A. Apostolidis, A. C. Huang, L. A. Vella; UPenn COVID Processing Unit, M. R. Betts, N. J. Meyer, E. J. Wherry, Deep immune profiling of COVID-19 patients reveals distinct immunotypes with therapeutic implications. *Science* **369**, eabc8511 (2020).

13. C. Rydyznski Moderbacher, S. Ramirez, J. Dan, A. Grifoni, K. Hastie, D. Weiskopf, S. Belanger, R. Abbott, C. Kim, J. Choi, Y. Kato, E. Crotty, C. Kim, S. Rawlings, J. Mateus, L. Tse, A. Frazier, R. Baric, B. Peters, J. Greenbaum, E. Ollmann Saphire, D. Smith, A. Sette,

S. Crotty, Antigen-specific adaptive immunity to SARS-CoV-2 in acute COVID-19 and associations with age and disease severity. *Cell* **183**, 996–1012.e19 (2020).

14. J. Y. Zhang, X. M. Wang, X. Xing, Z. Xu, C. Zhang, J. W. Song, X. Fan, P. Xia, J. L. Fu, S. Y. Wang, R. N. Xu, X. P. Dai, L. Shi, L. Huang, T. J. Jiang, M. Shi, Y. Zhang, A. Zumla, M. Maeurer, F. Bai, F. S. Wang, Single-cell landscape of immunological responses in patients with COVID-19. *Nat. Immunol.* **21**, 1107–1118 (2020).

15. W. Wen, W. Su, H. Tang, W. Le, X. Zhang, Y. Zheng, X. Liu, L. Xie, J. Li, J. Ye, L. Dong, X. Cui, Y. Miao, D. Wang, J. Dong, C. Xiao, W. Chen, H. Wang, Immune cell profiling of COVID-19 patients in the recovery stage by single-cell sequencing. *Cell Discov.* **6**, 31 (2020).

16. Y. Su, D. Chen, D. Yuan, C. Lausted, J. Choi, C. L. Dai, V. Voillet, V. R. Duvvuri, K. Scherler, P. Troisch, P. Baloni, G. Qin, B. Smith, S. A. Kornilov, C. Rostomily, A. Xu, J. Li, S. Dong, A. Rothchild, J. Zhou, K. Murray, R. Edmark, S. Hong, J. E. Heath, J. Earls, R. Zhang, J. Xie, S. Li, R. Roper, L. Jones, Y. Zhou, L. Rowen, R. Liu, S. Mackay, D. S. O'Mahony, C. R. Dale, J. A. Wallick, H. A. Algren, M. A. Zager; ISB-Swedish COVID19 Biobanking Unit, W. Wei, N. D. Price, S. Huang, N. Subramanian, K. Wang, A. T. Magis, J. J. Hadlock, L. Hood, A. Aderem, J. A. Bluestone, L. L. Lanier, P. D. Greenberg, R. Gottardo, M. M. Davis, J. D. Goldman, J. R. Heath, Multi-omics resolves a sharp disease-state shift between mild and moderate COVID-19. *Cell* **183**, 1479–1495.e20 (2020).

17. M. Liao, Y. Liu, J. Yuan, Y. Wen, G. Xu, J. Zhao, L. Cheng, J. Li, X. Wang, F. Wang, L. Liu, I. Amit, S. Zhang, Z. Zhang, Single-cell landscape of bronchoalveolar immune cells in patients with COVID-19. *Nat. Med.* **26**, 842–844 (2020).

18. L. Zhu, P. Yang, Y. Zhao, Z. Zhuang, Z. Wang, R. Song, J. Zhang, C. Liu, Q. Gao, Q. Xu, X. Wei, H.-X. Sun, B. Ye, Y. Wu, N. Zhang, G. Lei, L. Yu, J. Yan, G. Diao, F. Meng, C. Bai, P. Mao, Y. Yu, M. Wang, Y. Yuan, Q. Deng, Z. Li, Y. Huang, G. Hu, Y. Liu, X. Wang, Z. Xu, P. Liu, Y. Bi, Y. Shi, S. Zhang, Z. Chen, J. Wang, X. Xu, G. Wu, F.-S. Wang, G. F. Gao, L. Liu, W. J. Liu, Single-cell sequencing of peripheral mononuclear cells reveals distinct immune response landscapes of COVID-19 and influenza patients. *Immunity* **53**, 685–696.e3 (2020).

19. J. S. Lee, S. Park, H. W. Jeong, J. Y. Ahn, S. J. Choi, H. Lee, B. Choi, S. K. Nam, M. Sa, J. S. Kwon, S. J. Jeong, H. K. Lee, S. H. Park, S. H. Park, J. Y. Choi, S. H. Kim, I. Jung, E. C. Shin, Immunophenotyping of COVID-19 and influenza highlights the role of type I interferons in development of severe COVID-19. *Sci. Immunol.* **5**, eabd1554 (2020).

20. A. J. Wilk, A. Rustagi, N. Q. Zhao, J. Roque, G. J. Martinez-Colon, J. L. McKechnie, G. T. Ivison, T. Ranganath, R. Vergara, T. Hollis, L. J. Simpson, P. Grant, A. Subramanian, A. J. Rogers, C. A. Blish, A single-cell atlas of the peripheral immune response in patients with severe COVID-19. *Nat. Med.* **26**, 1070–1076 (2020).

21. P. B. Narasimhan, P. Marcovecchio, A. A. J. Hamers, C. C. Hedrick, Nonclassical monocytes in health and disease. *Annu. Rev. Immunol.* **37**, 439–456 (2019).

22. F. Venet, J. Demaret, M. Gossez, G. Monneret, Myeloid cells in sepsis-acquired immunodeficiency. *Ann. N. Y. Acad. Sci.* 10.1111/nyas.14333 , (2020).

23. E. M. Mace, J. S. Orange, Emerging insights into human health and NK cell biology from the study of NK cell deficiencies. *Immunol. Rev.* **287**, 202–225 (2019).

24. A. G. Freud, B. L. Mundy-Bosse, J. Yu, M. A. Caligiuri, The broad spectrum of human natural killer cell diversity. *Immunity* **47**, 820–833 (2017).

25. S. L. Smith, P. R. Kennedy, K. B. Stacey, J. D. Worboys, A. Yarwood, S. Seo, E. H. Solloa, B. Mistretta, S. S. Chatterjee, P. Gunaratne, K. Allette, Y. C. Wang, M. L. Smith, R. Sebra, E. M. Mace, A. Horowitz, W. Thomson, P. Martin, S. Eyre, D. M. Davis, Diversity of peripheral blood human NK cells identified by single-cell RNA sequencing. *Blood Adv.* **4**, 1388–1406 (2020).

26. C. Yang, J. R. Siebert, R. Burns, Z. J. Gerbec, B. Bonacci, A. Rymaszewski, M. Rau, M. J. Riese, S. Rao, K. S. Carlson, J. M. Routes, J. W. Verbsky, M. S. Thakar, S. Malarkannan, Heterogeneity of human bone marrow and blood natural killer cells defined by single-cell transcriptome. *Nat. Commun.* **10**, 3931 (2019).

27. S. Moir, A. S. Fauci, B-cell exhaustion in HIV infection: The role of immune activation. *Curr. Opin. HIV AIDS* **9**, 472–477 (2014).

28. R. T. Sullivan, C. C. Kim, M. F. Fontana, M. E. Feeney, P. Jagannathan, M. J. Boyle, C. J. Drakeley, I. Ssewanyana, F. Nankya, H. Mayanja-Kizza, G. Dorsey, B. Greenhouse, FCRL5 delineates functionally impaired memory B Cells associated with plasmodium falciparum exposure. *PLOS Pathog.* **11**, e1004894 (2015).

29. S. L. Peng, S. J. Szabo, L. H. Glimcher, T-bet regulates IgG class switching and pathogenic autoantibody production. *Proc. Natl. Acad. Sci. U.S.A.* **99**, 5545–5550 (2002).

30. A. A. Sheikh, L. Cooper, M. Feng, F. Souza-Fonseca-Guimaraes, F. Lafouresse, B. C. Duckworth, N. D. Huntington, J. J. Moon, M. Pellegrini, S. L. Nutt, G. T. Belz, K. L. Good-Jacobson, J. R. Groom, Context-dependent role for T-bet in T follicular helper differentiation and germinal center function following viral infection. *Cell Rep.* **28**, 1758–1772.e4 (2019).

31. J. P. Coutelier, J. T. van der Logt, F. W. Heessen, G. Warnier, J. Van Snick, IgG2a restriction of murine antibodies elicited by viral infections. *J. Exp. Med.* **165**, 64–69 (1987).

32. C. D. Peacock, S. K. Kim, R. M. Welsh, Attrition of virus-specific memory CD8+ T cells during reconstitution of lymphopenic environments. *J. Immunol.* **171**, 655–663 (2003).

33. J. M. McNally, C. C. Zarozinski, M. Y. Lin, M. A. Brehm, H. D. Chen, R. M. Welsh, Attrition of bystander CD8 T cells during virus-induced T-cell and interferon responses. *J. Virol.* **75**, 5965–5976 (2001).

34. F. Sallusto, D. Lenig, R. Forster, M. Lipp, A. Lanzavecchia, Two subsets of memory T lymphocytes with distinct homing potentials and effector functions. *Nature* **401**, 708–712 (1999).

35. R. A. Warnock, S. Askari, E. C. Butcher, U. H. von Andrian, Molecular mechanisms of lymphocyte homing to peripheral lymph nodes. *J. Exp. Med.* **187**, 205–216 (1998).

36. T. Willinger, T. Freeman, M. Herbert, H. Hasegawa, A. J. McMichael, M. F. Callan, Human naive CD8 T cells down-regulate expression of the WNT pathway transcription factors lymphoid enhancer binding factor 1 and transcription factor 7 (T cell factor-1) following antigen encounter in vitro and in vivo. *J. Immunol.* **176**, 1439–1446 (2006).

37. D. E. Speiser, M. Migliaccio, M. J. Pittet, D. Valmori, D. Lienard, F. Lejeune, P. Reichenbach, P. Guillaume, I. Luscher, J. C. Cerottini, P. Romero, Human CD8+ T cells expressing HLA-DR and CD28 show telomerase activity and are distinct from cytolytic effector T cells. *Eur. J. Immunol.* **31**, 459–466 (2001).

38. C. Zhong, C. Li, X. Wang, T. Toyoda, G. Gao, Z. Fan, Granzyme K inhibits replication of influenza virus through cleaving the nuclear transport complex importin α1/β dimer of infected host cells. *Cell Death Differ.* **19**, 882–890 (2012).

39. K. M. Hertoghs, P. D. Moerland, A. van Stijn, E. B. Remmerswaal, S. L. Yong, P. J. van de Berg, S. M. van Ham, F. Baas, I. J. ten Berge, R. A. van Lier, Molecular profiling of cytomegalovirus-induced human CD8+ T cell differentiation. *J. Clin. Invest.* **120**, 4077–4090 (2010).

40. A. Harari, F. Bellutti Enders, C. Cellerai, P.-A. Bart, G. Pantaleo, Distinct profiles of cytotoxic granules in memory CD8 T cells correlate with function, differentiation stage, and antigen exposure. *J. Virol.* **83**, 2862–2871 (2009).

41. C. Gerlach, E. A. Moseman, S. M. Loughhead, D. Alvarez, A. J. Zwijnenburg, L. Waanders, R. Garg, J. C. de la Torre, U. H. von Andrian, The chemokine receptor CX3CR1 defines three antigen-experienced CD8 T cell subsets with distinct roles in immune surveillance and homeostasis. *Immunity* **45**, 1270–1284 (2016).

42. L. M. Snell, B. L. MacLeod, J. C. Law, I. Osokine, H. J. Elsaesser, K. Hezaveh, R. J. Dickson, M. A. Gavin, C. J. Guidos, T. L. McGaha, D. G. Brooks, CD8+ T cell priming in established chronic viral infection preferentially directs differentiation of memory-like cells for sustained immunity. *Immunity* **49**, 678–694.e5 (2018).

43. T. Sekine, A. Perez-Potti, O. Rivera-Ballesteros, K. Strålin, J. Gorin, A. Olsson, S. Llewellyn-Lacey, H. Kamal, G. Bogdanovic, S. Muschiol, D. Wullimann, T. Kammann, J. Emgård, T. Parrot, E. Folkesson, O. Rooyackers, L. Eriksson, J. Henter, A. Sönnerborg, T. Allander, J. Albert, M. Nielsen, J. Klingström, S. Gredmark-Russ, N. Björkström, J. Sandberg, D. Price, H. Ljunggren, S. Aleman, M. Buggert; Karolinska COVID-19 Study Group, Robust T cell immunity in convalescent individuals with asymptomatic or mild COVID-19. *Cell* **183**, 158–168.e14 (2020).

44. R. S. Akondy, M. Fitch, S. Edupuganti, S. Yang, H. T. Kissick, K. W. Li, B. A. Youngblood, H. A. Abdelsamed, D. J. McGuire, K. W. Cohen, G. Alexe, S. Nagar, M. M. McCausland, S. Gupta, P. Tata, W. N. Haining, M. J. McElrath, D. Zhang, B. Hu, W. J. Greenleaf, J. J. Goronzy, M. J. Mulligan, M. Hellerstein, R. Ahmed, Origin and differentiation of human memory CD8 T cells after vaccination. *Nature* **552**, 362–367 (2017).

45. S. Sarkar, V. Kalia, W. N. Haining, B. T. Konieczny, S. Subramaniam, R. Ahmed, Functional and genomic profiling of effector CD8 T cell subsets with distinct memory fates. *J. Exp. Med.* **205**, 625–640 (2008).

46. R. Reantragoon, A. J. Corbett, I. G. Sakala, N. A. Gherardin, J. B. Furness, Z. Chen, S. B. Eckle, A. P. Uldrich, R. W. Birkinshaw, O. Patel, L. Kostenko, B. Meehan, K. Kedzierska, L. Liu, D. P. Fairlie, T. H. Hansen, D. I. Godfrey, J. Rossjohn, J. McCluskey, L. Kjer-Nielsen, Antigen-loaded MR1 tetramers define T cell receptor heterogeneity in mucosal-associated invariant T cells. *J. Exp. Med.* **210**, 2305–2320 (2013).

47. J. R. Fergusson, K. E. Smith, V. M. Fleming, N. Rajoriya, E. W. Newell, R. Simmons, E. Marchi, S. Bjorkander, Y. H. Kang, L. Swadling, A. Kurioka, N. Sahgal, H. Lockstone, D. Baban, G. J. Freeman, E. Sverremark-Ekstrom, M. M. Davis, M. P. Davenport, V. Venturi, J. E. Ussher, C. B. Willberg, P. Klenerman, CD161 defines a transcriptional and functional phenotype across distinct human T cell lineages. *Cell Rep.* **9**, 1075–1088 (2014).

48. R. Lamichhane, M. Schneider, S. M. de la Harpe, T. W. R. Harrop, R. F. Hannaway, P. K. Dearden, J. R. Kirman, J. D. A. Tyndall, A. J. Vernall, J. E. Ussher, TCR- or cytokine-activated CD8+ mucosal-associated invariant T cells are rapid polyfunctional effectors that can coordinate immune responses. *Cell Rep.* **28**, 3061–3076.e5 (2019).

49. A. Banerjee, A. S. Banks, M. C. Nawijn, X. P. Chen, P. B. Rothman, Cutting edge: Suppressor of cytokine signaling 3 inhibits activation of NFATp. *J. Immunol.* **168**, 4277–4281 (2002).

50. D. C. Palmer, N. P. Restifo, Suppressors of cytokine signaling (SOCS) in T cell differentiation, maturation, and function. *Trends Immunol.* **30**, 592–602 (2009).

51. J. T. Chang, E. J. Wherry, A. W. Goldrath, Molecular regulation of effector and memory T cell differentiation. *Nat. Immunol.* **15**, 1104–1115 (2014).

52. T. Ahrends, J. Busselaar, T. M. Severson, N. Babala, E. de Vries, A. Bovens, L. Wessels, F. van Leeuwen, J. Borst, CD4+ T cell help creates memory CD8+ T cells with innate and help-independent recall capacities. *Nat. Commun.* **10**, 5531 (2019).

53. D. Herndler-Brandstetter, H. Ishigame, R. Shinnakasu, V. Plajer, C. Stecher, J. Zhao, M. Lietzenmayer, L. Kroehling, A. Takumi, K. Kometani, T. Inoue, Y. Kluger, S. M. Kaech, T. Kurosaki, T. Okada, R. A. Flavell, KLRG1+ effector CD8+ T cells lose KLRG1, differentiate into all memory T cell lineages, and convey enhanced protective immunity. *Immunity* **48**, 716–729.e8 (2018).

54. R. He, S. Hou, C. Liu, A. Zhang, Q. Bai, M. Han, Y. Yang, G. Wei, T. Shen, X. Yang, L. Xu, X. Chen, Y. Hao, P. Wang, C. Zhu, J. Ou, H. Liang, T. Ni, X. Zhang, X. Zhou, K. Deng, Y. Chen, Y. Luo, J. Xu, H. Qi, Y. Wu, L. Ye, Follicular CXCR5- expressing CD8+ T cells curtail chronic viral infection. *Nature* **537**, 412–416 (2016).

55. Y. A. Leong, Y. Chen, H. S. Ong, D. Wu, K. Man, C. Deleage, M. Minnich, B. J. Meckiff, Y. Wei, Z. Hou, D. Zotos, K. A. Fenix, A. Atnerkar, S. Preston, J. G. Chipman, G. J. Beilman, C. C. Allison, L. Sun, P. Wang, J. Xu, J. G. Toe, H. K. Lu, Y. Tao, U. Palendira, A. L. Dent, A. L. Landay, M. Pellegrini, I. Comerford, S. R. McColl, T. W. Schacker, H. M. Long, J. D. Estes, M. Busslinger, G. T. Belz, S. R. Lewin, A. Kallies, D. Yu, CXCR5+ follicular cytotoxic T cells control viral infection in B cell follicles. *Nat. Immunol.* **17**, 1187–1196 (2016).

56. G. La Manno, R. Soldatov, A. Zeisel, E. Braun, H. Hochgerner, V. Petukhov, K. Lidschreiber, M. E. Kastriti, P. Lonnerberg, A. Furlan, J. Fan, L. E. Borm, Z. Liu, D. van Bruggen, J. Guo, X. He, R. Barker, E. Sundstrom, G. Castelo-Branco, P. Cramer, I. Adameyko, S. Linnarsson, P. V. Kharchenko, RNA velocity of single cells. *Nature* **560**, 494–498 (2018).

57. C. Huang, Y. Wang, X. Li, L. Ren, J. Zhao, Y. Hu, L. Zhang, G. Fan, J. Xu, X. Gu, Z. Cheng, T. Yu, J. Xia, Y. Wei, W. Wu, X. Xie, W. Yin, H. Li, M. Liu, Y. Xiao, H. Gao, L. Guo, J. Xie, G. Wang, R. Jiang, Z. Gao, Q. Jin, J. Wang, B. Cao, Clinical features of patients infected with 2019 novel coronavirus in Wuhan, China. *Lancet* **395**, 497–506 (2020).

58. S. Varchetta, D. Mele, B. Oliviero, S. Mantovani, S. Ludovisi, A. Cerino, R. Bruno, A. Castelli, M. Mosconi, M. Vecchia, S. Roda, M. Sachs, C. Klersy, M. U. Mondelli, Unique immunological profile in patients with COVID-19. *Cell. Mol. Immunol.* **18**, 604–612 (2020).

59. A. Carfi, R. Bernabei, F. Landi; Gemelli Against COVID-19 Post-Acute Care Study Group, Persistent symptoms in patients after acute COVID-19. *JAMA* **324**, 603–605 (2020).

60. P. Bastard, L. B. Rosen, Q. Zhang, E. Michailidis, H. H. Hoffmann, Y. Zhang, K. Dorgham, Q. Philippot, J. Rosain, V. Beziat, J. Manry, E. Shaw, L. Haljasmagi, P. Peterson, L. Lorenzo, L. Bizien, S. Trouillet-Assant, K. Dobbs, A. A. de Jesus, A. Belot, A. Kallaste, E. Catherinot, Y. Tandjaoui-Lambiotte, J. Le Pen, G. Kerner, B. Bigio, Y. Seeleuthner, R. Yang, A. Bolze, A. N. Spaan, O. M. Delmonte, M. S. Abers, A. Aiuti, G. Casari, V. Lampasona, L. Piemonti, F. Ciceri, K. Bilguvar, R. P. Lifton, M. Vasse, D. M. Smadja, M. Migaud, J. Hadjadj, B. Terrier, D. Duffy, L. Quintana-Murci, D. van de Beek, L. Roussel, D. C. Vinh, S. G. Tangye, F. Haerynck, D. Dalmau, J. Martinez-Picado, P. Brodin, M. C. Nussenzweig, S. Boisson-Dupuis, C. Rodriguez-Gallego, G. Vogt, T. H. Mogensen, A. J. Oler, J. Gu, P. D. Burbelo, J. I. Cohen, A. Biondi, L. R. Bettini, M. D'Angio, P. Bonfanti, P. Rossignol, J. Mayaux, F. Rieux-Laucat, E. S. Husebye, F. Fusco, M. V. Ursini, L. Imberti, A. Sottini, S. Paghera, E. Quiros-Roldan, C. Rossi, R. Castagnoli, D. Montagna, A. Licari, G. L. Marseglia, X. Duval, J. Ghosn; HGID Lab; NIAID-USUHS Immune Response to COVID Group; COVID Clinicians; COVID-STORM Clinicians; Imagine COVID Group; French COVID Cohort Study Group; Milieu Intérieur Consortium; CoV-Contact Cohort; Amsterdam UMC Covid-19 Biobank; COVID Human Genetic Effort, J. S. Tsang, R. Goldbach-Mansky, K. Kisand, M. S. Lionakis, A. Puel, S. Y. Zhang, S. M. Holland, G. Gorochov, E. Jouanguy, C. M. Rice, A. Cobat, L. D. Notarangelo, L. Abel, H. C. Su, J. L. Casanova, Autoantibodies against type I IFNs in patients with life-threatening COVID-19. *Science* **370**, eabd4585 (2020).

61. Q. Zhang, P. Bastard, Z. Liu, J. Le Pen, M. Moncada-Velez, J. Chen, M. Ogishi, I. K. D. Sabli, S. Hodeib, C. Korol, J. Rosain, K. Bilguvar, J. Ye, A. Bolze, B. Bigio, R. Yang, A. A. Arias, Q. Zhou, Y. Zhang, F. Onodi, S. Korniotis, L. Karpf, Q. Philippot, M. Chbihi, L. Bonnet-Madin, K. Dorgham, J. E. Han, L. Lorenzo, L. Bizien, P. Meade, A. L. Neehus, A. C. Ugurbil, A. Corneau, G. Kerner, P. Zhang, F. Rapaport, Y. Seeleuthner, J. Manry, C. Masson, Y. Schmitt, A. Schluter, T. Le Voyer, T. Khan, J. Li, J. Fellay, L. Roussel, M. Shahrooei, M. F. Alosaimi, D. Mansouri, H. Al-Saud, F. Al-Mulla, F. Almourfi, S. Z. Al-Muhsen, F. Alsohime, S. Al Turki, R. Hasanato, D. van de Beek, A. Biondi, L. R. Bettini, M. D'Angio, P. Bonfanti, L. Imberti, A. Sottini, S. Paghera, E. Quiros-Roldan, C. Rossi, A. J. Oler, M. F. Tompkins, C. Alba, I. Vandernoot, J. C. Goffard, G. Smits, I. Migeotte, F. Haerynck, P. Soler-Palacin, A. Martin-Nalda, R. Colobran, P. E. Morange, S. Keles, F. Colkesen, T. Ozcelik, K. K. Yasar, S. Senoglu, S. N. Karabela, C. Rodriguez-Gallego, G. Novelli, S. Hraiech, Y. Tandjaoui-Lambiotte, X. Duval, C. Laouénan; COVID-STORM Clinicians; COVID Clinicians; Imagine COVID Group; French COVID Cohort Study Group; CoV-Contact Cohort; Amsterdam UMC Covid-19 Biobank; COVID Human Genetic Effort; NIAID-USUHS/TAGC COVID Immunity Group, A. L. Snow, C. L. Dalgard, J. D. Milner, D. C. Vinh, T. H. Mogensen, N. Marr, A. N. Spaan, B. Boisson, S. Boisson-Dupuis, J. Bustamante, A. Puel, M. J. Ciancanelli, I. Meyts, T. Maniatis, V. Soumelis, A. Amara, M. Nussenzweig, A. Garcia-Sastre, F. Krammer, A. Pujol, D. Duffy, R. P. Lifton, S. Y. Zhang, G. Gorochov, V. Beziat, E. Jouanguy, V. Sancho-Shimizu, C. M. Rice, L. Abel, L. D. Notarangelo, A. Cobat, H. C. Su, J. L. Casanova, Inborn errors of type I IFN immunity in patients with life-threatening COVID-19. *Science* **370**, eabd4570 (2020).

62. D. Blanco-Melo, B. E. Nilsson-Payant, W. C. Liu, S. Uhl, D. Hoagland, R. Moller, T. X. Jordan, K. Oishi, M. Panis, D. Sachs, T. T. Wang, R. E. Schwartz, J. K. Lim, R. A. Albrecht, B. R. tenOever, Imbalanced host response to SARS-CoV-2 drives development of COVID-19. *Cell* **181**, 1036–1045.e9 (2020).

63. J. Hadjadj, N. Yatim, L. Barnabei, A. Corneau, J. Boussier, N. Smith, H. Pere, B. Charbit, V. Bondet, C. Chenevier-Gobeaux, P. Breillat, N. Carlier, R. Gauzit, C. Morbieu, F. Pene, N. Marin, N. Roche, T. A. Szwebel, S. H. Merkling, J. M. Treluyer, D. Veyer, L. Mouthon, C. Blanc, P. L. Tharaux, F. Rozenberg, A. Fischer, D. Duffy, F. Rieux-Laucat, S. Kerneis, B. Terrier, Impaired type I interferon activity and inflammatory responses in severe COVID-19 patients. *Science* **369**, 718–724 (2020).

64. E. J. Giamarellos-Bourboulis, M. G. Netea, N. Rovina, K. Akinosoglou, A. Antoniadou, N. Antonakos, G. Damoraki, T. Gkavogianni, M. E. Adami, P. Katsaounou, M. Ntaganou, M. Kyriakopoulou, G. Dimopoulos, I. Koutsodimitropoulos, D. Velissaris, P. Koufargyris, A. Karageorgos, K. Katrini, V. Lekakis, M. Lupse, A. Kotsaki, G. Renieris, D. Theodoulou, V. Panou, E. Koukaki, N. Koulouris, C. Gogos, A. Koutsoukou, Complex immune dysregulation in COVID-19 patients with severe respiratory failure. *Cell Host Microbe* **27**, 992–1000.e3 (2020).

65. J. Schulte-Schrepping, N. Reusch, D. Paclik, K. Baßler, S. Schlickeiser, B. Zhang, B. Krämer, T. Krammer, S. Brumhard, L. Bonaguro, E. De Domenico, D. Wendisch, M. Grasshoff, T. S. Kapellos, M. Beckstette, T. Pecht, A. Saglam, O. Dietrich, H. E. Mei, A. R. Schulz, C. Conrad, D. Kunkel, E. Vafadarnejad, C.-J. Xu, A. Horne, M. Herbert, A. Drews, C. Thibeault, M. Pfeiffer, S. Hippenstiel, A. Hocke, H. Müller-Redetzky, K.-M. Heim, F. Machleidt, A. Uhrig, L. B. de Jarcy, J. Jürgens, M. Stegemann, C. R. Glösenkamp, H.-D. Volk, C. Goffinet, M. Landthaler, E. Wyler, P. Georg, M. Schneider, C. Dang-Heine, N. Neuwinger, K. Kappert, R. Tauber, V. Corman, J. Raabe, K. M. Kaiser, M. T. Vinh, G. Rieke, C. Meisel, T. Ulas, M. Becker, R. Geffers, M. Witzenrath, C. Drosten, N. Suttorp, C. von Kalle, F. Kurth, K. Händler, J. L. Schultze, A. C. Aschenbrenner, Y. Li, J. Nattermann, B. Sawitzki, A.-E. Saliba, L. E. Sander; Deutsche COVID-19 OMICS Initiative (DeCOI), Severe COVID-19 is marked by a dysregulated myeloid cell compartment. *Cell* **182**, 1419–1440.e23 (2020).

66. Y. Wang, L. Zhang, L. Sang, F. Ye, S. Ruan, B. Zhong, T. Song, A. N. Alshukairi, R. Chen, Z. Zhang, M. Gan, A. Zhu, Y. Huang, L. Luo, C. K. P. Mok, M. M. Al Gethamy, H. Tan, Z. Li, X. Huang, F. Li, J. Sun, Y. Zhang, L. Wen, Y. Li, Z. Chen, Z. Zhuang, J. Zhuo, C. Chen, L. Kuang, J. Wang, H. Lv, Y. Jiang, M. Li, Y. Lin, Y. Deng, L. Tang, J. Liang, J. Huang, S. Perlman, N. Zhong, J. Zhao, J. S. M. Peiris, Y. Li, J. Zhao, Kinetics of viral load and antibody response in relation to COVID-19 severity. *J. Clin. Invest.* **130**, 5235–5244 (2020).

67. L. Piccoli, Y.-J. Park, M. A. Tortorici, N. Czudnochowski, A. C. Walls, M. Beltramello, C. Silacci-Fregni, D. Pinto, L. E. Rosen, J. E. Bowen, O. J. Acton, S. Jaconi, B. Guarino, A. Minola, F. Zatta, N. Sprugasci, J. Bassi, A. Peter, A. De Marco, J. C. Nix, F. Mele, S. Jovic, B. F. Rodriguez, S. V. Gupta, F. Jin, G. Piumatti, G. L. Presti, A. F. Pellanda, M. Biggiogero, M. Tarkowski, M. S. Pizzuto, E. Cameroni, C. Havenar-Daughton, M. Smithey, D. Hong, V. Lepori, E. Albanese, A. Ceschi, E. Bernasconi, L. Elzi, P. Ferrari, C. Garzoni, A. Riva, G. Snell, F. Sallusto, K. Fink, H. W. Virgin, A. Lanzavecchia, D. Corti, D. Veesler, Mapping neutralizing and immunodominant sites on the SARS-CoV-2 spike receptor-binding domain by structure-guided high-resolution serology. *Cell* **183**, 1024–1042.e21 (2020).

68. L. Premkumar, B. Segovia-Chumbez, R. Jadi, D. R. Martinez, R. Raut, A. Markmann, C. Cornaby, L. Bartelt, S. Weiss, Y. Park, C. E. Edwards, E. Weimer, E. M. Scherer, N. Rouphael, S. Edupuganti, D. Weiskopf, L. V. Tse, Y. J. Hou, D. Margolis, A. Sette, M. H. Collins, J. Schmitz, R. S. Baric, A. M. de Silva, The receptor binding domain of the viral spike protein is an immunodominant and highly specific target of antibodies in SARS-CoV-2 patients. *Sci. Immunol.* **5**, eabc8413 (2020).

69. H. Q. Yu, B. Q. Sun, Z. F. Fang, J. C. Zhao, X. Y. Liu, Y. M. Li, X. Z. Sun, H. F. Liang, B. Zhong, Z. F. Huang, P. Y. Zheng, L. F. Tian, H. Q. Qu, D. C. Liu, E. Y. Wang, X. J. Xiao, S. Y. Li, F. Ye, L. Guan, D. S. Hu, H. Hakonarson, Z. G. Liu, N. S. Zhong, Distinct features of SARS-CoV-2-specific IgA response in COVID-19 patients. *Eur. Respir. J.* **56**, 2001526 (2020).

70. B. Oliviero, S. Varchetta, D. Mele, S. Mantovani, A. Cerino, C. G. Perotti, S. Ludovisi, M. U. Mondelli, Expansion of atypical memory B cells is a prominent feature of COVID-19. *Cell. Mol. Immunol.* **17**, 1101–1103 (2020).

71. C. O. Ogega, N. E. Skinner, P. W. Blair, H. S. Park, K. Littlefield, A. Ganesan, S. Dhakal, P. Ladiwala, A. A. Antar, S. C. Ray, M. J. Betenbaugh, A. Pekosz, S. L. Klein, Y. C. Manabe, A. L. Cox, J. R. Bailey, Durable SARS-CoV-2 B cell immunity after mild or severe disease. *J. Clin. Invest.* **131**, e145516 (2021).

72. C. C. Kim, A. M. Baccarella, A. Bayat, M. Pepper, M. F. Fontana, FCRL5+ memory B cells exhibit robust recall responses. *Cell Rep.* **27**, 1446–1460.e4 (2019).

73. N. Dauby, C. Kummert, S. Lecomte, C. Liesnard, M. L. Delforge, C. Donner, A. Marchant, Primary human cytomegalovirus infection induces the expansion of virus-specific activated and atypical memory B cells. *J. Infect. Dis.* **210**, 1275–1285 (2014).

74. A. J. Gerth, L. Lin, S. L. Peng, T-bet regulates T-independent IgG2a class switching. *Int. Immunol.* **15**, 937–944 (2003).

75. K. Rubtsova, A. V. Rubtsov, L. F. van Dyk, J. W. Kappler, P. Marrack, T-box transcription factor T-bet, a key player in a unique type of B-cell activation essential for effective viral clearance. *Proc. Natl. Acad. Sci. U.S.A.* **110**, E3216–E3224 (2013).

76. E. Szomolanyi-Tsuda, R. M. Welsh, T-cell-independent antiviral antibody responses. *Curr. Opin. Immunol.* **10**, 431–435 (1998).

77. R. M. Welsh, L. K. Selin, E. Szomolanyi-Tsuda, Immunological memory to viral infections. *Annu. Rev. Immunol.* **22**, 711–743 (2004).

78. J. R. Teijaro, D. Turner, Q. Pham, E. J. Wherry, L. Lefrancois, D. L. Farber, Cutting edge: Tissue-retentive lung memory CD4 T cells mediate optimal protection to respiratory virus infection. *J. Immunol.* **187**, 5510–5514 (2011).

79. C. K. Li, H. Wu, H. Yan, S. Ma, L. Wang, M. Zhang, X. Tang, N. J. Temperton, R. A. Weiss, J. M. Brenchley, D. C. Douek, J. Mongkolsapaya, B. H. Tran, C. L. Lin, G. R. Screaton, J. L. Hou, A. J. McMichael, X. N. Xu, T cell responses to whole SARS coronavirus in humans. *J. Immunol.* **181**, 5490–5500 (2008).

80. A. Lombardi, E. Trombetta, A. Cattaneo, V. Castelli, E. Palomba, M. Tirone, D. Mangioni, G. Lamorte, M. Manunta, D. Prati, F. Ceriotti, R. Gualtierotti, G. Costantino, S. Aliberti, V. Scaravilli, G. Grasselli, A. Gori, L. Porretti, A. Bandera, Early phases of COVID-19 are characterized by a reduction in lymphocyte populations and the presence of atypical monocytes. *Front. Immunol.* **11**, 560330 (2020).

81. M. B. Graham, V. L. Braciale, T. J. Braciale, Influenza virus-specific CD4+ T helper type 2 T lymphocytes do not promote recovery from experimental virus infection. *J. Exp. Med.* **180**, 1273–1282 (1994).

82. S. I. Jeong, J. W. Kim, K. P. Ko, B. K. Ryu, M. G. Lee, H. J. Kim, S. G. Chi, XAF1 forms a positive feedback loop with IRF-1 to drive apoptotic stress response and suppress tumorigenesis. *Cell Death Dis.* **9**, 806 (2018).

83. C. Schultheß, L. Paschold, D. Simnica, M. Mohme, E. Willscher, R. von Wenserski, R. Scholz, I. Wieters, C. Dahlke, E. Tolosa, D. G. Sedding, S. Ciesek, M. Addo, M. Binder, Next-generation sequencing of T and B cell receptor repertoires from COVID-19 patients showed signatures associated with severity of disease. *Immunity* **53**, 442–455.e4 (2020).

84. A. A. Minervina, M. V. Pogorelyy, E. A. Komech, V. K. Karnaukhov, P. Bacher, E. Rosati, A. Franke, D. M. Chudakov, I. Z. Mamedov, Y. B. Lebedev, T. Mora, A. M. Walczak, Primary and secondary anti-viral response captured by the dynamics and phenotype of individual T cell clones. *eLife* **9**, e53704 (2020).

85. L. Kjer-Nielsen, O. Patel, A. J. Corbett, J. Le Nours, B. Meehan, L. Liu, M. Bhati, Z. Chen, L. Kostenko, R. Reantragoon, N. A. Williamson, A. W. Purcell, N. L. Dudek, M. J. McConville, R. A. O'Hair, G. N. Khairallah, D. I. Godfrey, D. P. Fairlie, J. Rossjohn, J. McCluskey, MR1 presents microbial vitamin B metabolites to MAIT cells. *Nature* **491**, 717–723 (2012).

86. B. van Wilgenburg, I. Scherwitzl, E. C. Hutchinson, T. Leng, A. Kurioka, C. Kulicke, C. de Lara, S. Cole, S. Vasanawathana, W. Limpitikul, P. Malasit, D. Young, L. Denney; STOP-HCV consortium, M. D. Moore, P. Fabris, M. T. Giordani, Y. H. Oo, S. M. Laidlaw, L. B. Dustin, L. P. Ho, F. M. Thompson, N. Ramamurthy, J. Mongkolsapaya, C. B. Willberg, G. R. Screaton, P. Klenerman, MAIT cells are activated during human viral infections. *Nat. Commun.* **7**, 11653 (2016).

87. F. Tang, Y. Quan, Z. T. Xin, J. Wrammert, M. J. Ma, H. Lv, T. B. Wang, H. Yang, J. H. Richardus, W. Liu, W. C. Cao, Lack of peripheral memory B cell responses in recovered patients with severe acute respiratory syndrome: A six-year follow-up study. *J. Immunol.* **186**, 7264–7268 (2011).

88. J. M. Dan, J. Mateus, Y. Kato, K. M. Hastie, E. D. Yu, C. E. Faliti, A. Grifoni, S. I. Ramirez, S. Haupt, A. Frazier, C. Nakao, V. Rayaprolu, S. A. Rawlings, B. Peters, F. Krammer, V. Simon, E. O. Saphire, D. M. Smith, D. Weiskopf, A. Sette, S. Crotty, Immunological memory to SARS-CoV-2 assessed for up to 8 months after infection. *Science* **371**, eabf4063 (2021).

89. J. S. Turner, W. Kim, E. Kalaidina, C. W. Goss, A. M. Rauseo, A. J. Schmitz, L. Hansen, A. Haile, M. K. Klebert, I. Pusic, J. A. O'Halloran, R. M. Presti, A. H. Ellebedy, SARS-CoV-2 infection induces long-lived bone marrow plasma cells in humans. *Nature* **595**, 421–425 (2021).

90. Z. Wang, F. Muecksch, D. Schaefer-Babajew, S. Finkin, C. Viant, C. Gaebler, H. H. Hoffmann, C. O. Barnes, M. Cipolla, V. Ramos, T. Y. Oliveira, A. Cho, F. Schmidt, J. da Silva, E. Bednarski, L. Aguado, J. Yee, M. Daga, M. Turroja, K. G. Millard, M. Jankovic, A. Gazumyan, Z. Zhao, C. M. Rice, P. D. Bieniasz, M. Caskey, T. Hatziioannou, M. C. Nussenzweig, Naturally enhanced neutralizing breadth against SARS-CoV-2 one year after infection. *Nature* **595**, 426–431 (2021).

91. L. B. Rodda, J. Netland, L. Shehata, K. B. Pruner, P. A. Morawski, C. D. Thouvenel, K. K. Takehara, J. Eggenberger, E. A. Hemann, H. R. Waterman, M. L. Fahning, Y. Chen, M. Hale, J. Rathe, C. Stokes, S. Wrenn, B. Fiala, L. Carter, J. A. Hamerman, N. P. King, M. Gale Jr., D. J. Campbell, D. J. Rawlings, M. Pepper, Functional SARS-CoV-2-specific immune memory persists after mild COVID-19. *Cell* **184**, 169–183.e17 (2021).

92. Y. Zhang, L. Zheng, L. Zhang, X. Hu, X. Ren, Z. Zhang, Deep single-cell RNA sequencing data of individual T cells from treatment-naïve colorectal cancer patients. *Sci. Data* **6**, 131 (2019).